

Water and carbon fluxes in irrigated citrus orchards assessed from satellite data

December 2017

Author

Sergio Contreras
Johannes Hunink
Alain Baille

Client

Universidad Politécnica de Cartagena

FutureWater Report 174



FutureWater

Paseo Alfonso XIII, 48
30203 Cartagena (Murcia)
España

+34 868 071 286

info@futurewater.es

www.futurewater.es

Preface

Approximately 22 million tons of citrus crops, 20% of total world production, are produced in the Mediterranean region. Better quantitative knowledge on the environmental drivers that control water consumption, the productivity and the carbon footprint of these agrosystems are required to secure the sustainability of these cropping systems in the Mediterranean region.

The general aim of this study is to evaluate several satellite-based methods in combination with field data on water and carbon fluxes obtained in three Citrus commercial farms located in the Campo de Cartagena (Murcia, Spain).

FutureWater collaborated in this project and carried out the following tasks:

- 1) analyze the daily dynamics of water, energy and carbon in the selected pilot sites,
- 2) identify and quantify the influence of the main environmental drivers of water and carbon balance,
- 3) calibrate empirical relationships and production models for estimating actual evapotranspiration, and gross and net primary productivity gross, from field-based weather inputs, and satellite-based variables.

The authors would like to thank the Agroforestry department of the Universidad Politécnica de Cartagena, and especially Bernardo Martín-Gorriz, who has been the main responsible for the field data collection.

Table of contents

1	Introduction	6
1.1	Background and objective	6
1.2	Satellite-based crop evapotranspiration	6
1.3	Primary production models	8
2	Data and methods	11
2.1	Study area	11
2.2	Satellite data products	11
2.3	Ground-based energy and water balance measurements	13
2.4	Net primary production	14
3	Results and discussion	21
3.1	Analysis of field data	21
3.2	Energy and crop-coefficient dynamics	22
3.3	Calibration of empirical ET relationships	26
3.4	Light Use Efficiency: temporal variability	30
3.5	Satellite-based versus ground-based variables	34
3.6	Calibration of Production Efficiency Models	36
	3.6.1 VI model	36
	3.6.2 MOD-PCM model	38
4	Conclusions	40
5	References	41
	Appendix I: Satellite-based Production Efficiency Models	47
	5.1.1 CASA (Carnegie Ames Stanford Approach)	47
	5.1.2 SDBM (Simple Diagnostic Biosphere Model)	47
	5.1.3 TURC	48
	5.1.4 C-Fix	48
	5.1.5 3-PGS (3-Physiological Principles Predicting Growth using Satellites)	48
	5.1.6 GLO-PEM	49
	5.1.7 MOD17	49
	5.1.8 BEAMS (Biosphere model integrating Eco-physiological And Mechanistic approaches using Satellite data)	53
	5.1.9 EC-LUE model (Eddy Covariance – Light Use Efficiency model)	54
	5.1.10 VPM (Vegetation Photosynthesis Model)	55
	5.1.11 VI-based models for estimating GPP	56



Tables

Table 1. EC systems at the study area	11
Table 2. Satellite-based variables used in this study	12
Table 1. PEM models reviewed.....	17
Table 2. Comparison and performance analyses found in literature for Production Efficiency Models.....	20
Table 3. Average \pm standard errors of turbulent fluxes (LE=latent; H=sensible), Bowen ratio (H/LE), evaporative fraction (LE/(H+LE)) and crop coefficient (LE/E _{ref}). Statistics refer to the common measuring period. Statistical differences (***)=p-level<0.01) was detected using a t-test for dependent samples.....	24
Table 4. Pearson correlation coefficients (r) among energy balance traits and meteorological and satellite-based data computed daily. All correlations are significant, except those with the n.s. flag.....	27
Table 5. Pearson correlation coefficients (r) among energy balance traits and meteorological and satellite-based data computed at 8-day temporal windows. All correlations are significant, except those with the n.s. flag.....	28
Table 6. Predictive error parameters reported for the LE, and E _{ref} and LST _{a_D} relationships.....	29
Table 5. 90th-percentile values measured in Light Use Efficiencies at Citrus plots (days with negative NPP values were excluded in the analysis).	32
Table 6. Relationships between satellite-based variables and EC-based FPAR and LUE values.	35
Table 7. Pearson correlations (r values) between productivity values and satellite-based traits. LST refers to Day Land Surface Temperature retrieved by Terra platform. Pearson correlations consider a simple linear regression with intercept.	36
Table 3. Temperature thresholds used for computing the T-scalar parameter in the VPM model.	55

Figures

Figure 1. Study area.....	11
Figure 3. Retrieval of 8-day timeseries from 16-d composite values of vegetation indices.....	12
Figure 2. Outliers (red circles) excluded from the analysis.	14
Figure 1. Number of cites registered until 15-Feb-2016 in SCOPUS for each PEM-Diagnostic model.....	15
Figure 4. Standardized trajectories of field-based LAI measurements, and actual evapotranspiration (LE) and Gross Primary Production (GPP) observed at Villa Antonia from February-2010 to February-2011.	21
Figure 5. Standardized trajectories of field-based LAI measurements, and satellite-based vegetation indices (EVI and NDVI) observed at Villa Antonia from February-2010 to February-2011.....	22
Figure 6. Standardized trajectories of field-based LAI measurements, actual evapotranspiration (LE) and satellite-based Land Surface Temperature at midday (LST _d) observed at Villa Antonia from February-2010 to February-2011.	22
Figure 7. Daily turbulent fluxes (upper-left: latent heat, upper-right: sensible heat), and evaporative (lower-left) and crop coefficient (lower-right) values measured in experimental	

stations. Solid-black: Villa Antonia (VA); dashed-red: Casa Mulero (CM); blue line in lower-right panel defines the basal crop coefficient adopted for both systems.	23
Figure 8. 8-day averaged turbulent fluxes (upper-left: latent heat, upper-right: sensible heat), and evaporative (lower-left) and crop coefficient (lower-right) values measured in experimental stations. Solid-black: Villa Antonia (VA); dashed-red: Casa Mulero (CM); blue line in lower-right panel defines the basal crop coefficient adopted for both systems.	23
Figure 9. Sensible vs Latent heat fluxes scatterplot observed at VA and CM experimental stations.	24
Figure 10. Monthly boxplots of daily actual evapotranspiration (LE, left) and crop coefficients (k_c , right) measured in Villa Antonia and Casa Mulero experimental stations. Percentages represents the value of percentile taken.	25
Figure 11. Slopes of the E_{ref} -LE relationship (average crop coefficient) for VA (filled circles, solid line) and CM (open circles, dashed line). Dotted line shows the 95% prediction band for the overall pool of data.	26
Figure 13. Monthly variation of the relative RMSE (left-axis) between observed (right-axis) and predicted values of actual evapotranspiration.	29
Figure 14. LST-LE relationships at Villa-Antonia and Casa-Mulero experimental stations from daily (left) and 8-day values (right).	30
Figure 15. Threshold (P5 and P95 percentile) functions for the LSTd-crop coefficient relationship for VA and CM sites. Basal crop coefficient stated at 0.62.	30
Figure 7. Relationship between daily values of PAR and NEE at Villa Antonia (filled dots) and Casa Mulero (open dots).	32
Figure 8. Comparison of ground-based LAI measurements and FPAR estimates at Villa Antonia. FPAR values computed according Ogutu & Dash (Ogutu and Dash, 2013a).	32
Figure 9. Seasonal variation of gross and net LUE values in Villa Antonia (VA, filled dots) and Casa Mulero (CM, open dots) experimental stations.	33
Figure 10. Boxplots with seasonal differences in Light Use Efficiency values (LUE, gC/MJ) in Villa Antonia (VA) and Casa Mulero (CM) stations. Results retrieved from the 1d-timescale dataset.	34
Figure 11. Scatterplots between daytime Land Surface Temperature and EC-based FPAR and LUE estimates.	35
Figure 12. Matrix of scatterplots between productivity and LUE values, and satellite-based traits (alone or combined with PAR measurements). Relationships using the 8d-timescale dataset and taking the VA and CM values as a whole.	37
Figure 13. Seasonal dynamics of LST and productivity values at Villa Antonia (left) and Casa Mulero (right).	37
Figure 14. Calibration of no-intercept simple linear regression models for GPP estimation in Villa Antonia using PAR and NDVI as predictors. Calibration done using the 8-d timescale dataset.	38
Figure 2. Diagrammatic representation of the 3-PGS model (taken from Coops et al. (Coops et al., 1998)).	49
Figure 3. Conceptual structure of MOD17 algorithm (taken from Running and Zhao (Running and Zhao, 2015))	50
Figure 4. Schematic diagram of the BEAMS model (taken from Sasai et al. (Sasai et al., 2005)).	54
Figure 5. Input datasets used in BEAMS (taken from Sasai et al. (Sasai et al., 2005)).	54
Figure 6. Actual GPP measurements as a function of Land Surface Temperature (LST) in different vegetation-type systems (taken from Sims et al. (2008)).	57



1 Introduction

1.1 Background and objective

Approximately 22 million tons of citrus crops, 20% of total world production, are produced in the Mediterranean region. Historically, Citrus-dominated agrosystems have been concentrated in the valleys where the most fertile soils are located and a higher and easier access to surface or groundwater is possible. However, over the last decades, the adoption of new technologies and irrigation strategies (pressurized irrigation and deficit irrigation techniques) has promoted the expansion of the cropped areas to less favorable locations. Currently there are more than 300,000 hectares of citrus in Spain.

Better quantitative knowledge on the actual water requirements and the environmental drivers that control the productivity and the carbon footprint of these agrosystems are required to secure the sustainability of these cropping systems in the Mediterranean region. For this reason, during 5 years, the Agroforestry Engineering department of the Polytechnic University of Cartagena (UPCT) measured using the Eddy-covariance technique the water and carbon fluxes in three Citrus commercial farms located in the Campo de Cartagena (Murcia, Spain).

The main objective of this study is to quantify the water and carbon balance of Citrus orchards by combining satellite data and satellite-based methods with field and Eddy-covariance measurements. More specifically, the objectives are:

- 1) analyze the daily dynamics of water, energy and carbon in the selected pilot sites,
- 2) identify and quantify the influence of the main environmental drivers of water and carbon balance,
- 3) calibrate empirical relationships and production models for estimating actual evapotranspiration, and gross and net primary productivity gross, from field-based weather inputs, and satellite-based variables

Principle satellite variables studied are vegetation greenness and land surface water indices, albedo and land surface temperature.

1.2 Satellite-based crop evapotranspiration

Crop consumptive use, or actual evapotranspiration (ET_a), has been traditionally computed in agronomic applications according the standardized FAO guidelines for crop-water requirements described by Allen et al (1998), in which ET_a is estimated by an hypothetical potential flux, the “reference evapotranspiration (ET_{ref})” that can be derived from local meteorological observations, and a crop coefficient (K_c), i.e.

$$ET_a = K_c * ET_{ref}$$

Equation 1

Traditionally, K_c values have been tabulated for a large number of crops based on experiments in which crops have been grown under optimum agronomic conditions. The direct application of tabulated K_c values over agricultural lands tends to overestimate crop consumptive use when growth limiting conditions are present (Glenn et al., 2011). To account for these limiting conditions, scalar functions are commonly adopted for to compute actual crop coefficients (Pereira et al., 2014).

Satellite-based methods are an alternative and sometimes more adequate mean for providing regional-scale estimates of ET_a (Szilagyi, 2015) compared to the traditional FAO procedure or the relatively more expensive 'Bowen ratio' and 'Eddy covariance' ground-based techniques. They have the advantage that they can provide an indirect measure of the vegetative state of the crop and thus its evapotranspiration potential. Also these methods can be used for larger areas and can be relatively cost-efficient.

Satellite-based methods fall in two categories (Courault et al., 2005; Li et al., 2009):

- a) 'Surface Energy Balance' (SEB) methods which derive ET_a analytically as the residual among all the other energy fluxes accounted in the land (net radiation, sensible heat and ground heat) (Allen et al., 2011, 2007; Kalma et al., 2008), and
- b) 'Vegetation Index-Crop coefficient' (VI- K_c) methods which use VI as direct surrogates of the actual water consumption and growth dynamics of crops (Glenn et al., 2011; Kamble et al., 2013; Mateos et al., 2013; Nagler et al., 2013; Singh and Irmak, 2009).

Most of the derived-SEB algorithms found in literature (e.g. SEBAL, METRIC, S-SEB and METRIC, see Kalma et al. (Kalma et al., 2008) for a more detailed review) requires high-moderate resolution imagery (e.g. SPOT, ASTER, Landsat) in order to capture a sufficiently wide range of surface wetness conditions from which to parameterize the warm-cold edges along a bare-fully vegetated soil coverage gradient. Despite their generalized use, these methods are frequently difficult to calibrate and are also tied to high uncertainties and some degree of empiricism due to the assumptions adopted (Szilagyi, 2015). The low temporal and intermittent coverage of high-moderate spatial resolution satellites may additionally increase the difficulties in applying these methods and becoming them less attractive for operational applications (Glenn et al., 2010; Kalma et al., 2008).

VI-based methods have been evaluated over a large number of crop systems and have proved to be consistent under many conditions. VI values have been proposed as actual surrogates of K_c values, representing the actual performance of crops but also in irrigation scheduling applications (Bausch (1995) and references cited by Glenn et al. (Glenn et al., 2011)). They have also been found useful for basin-scale hydrological modeling (Hunink et al., 2017).

VI-based methods which use coarse-spatial resolution but high-temporal coverage imagery, as those provided by the MODIS sensors on Terra and Aqua satellite platforms have been found useful for operational applications to quantify crop ET_a (Contreras et al., 2014; Glenn et al., 2011; Hunink et al., 2015). VI- K_c methods have two main limitations:

- 1) they do not account direct evaporation losses accounted after rainfall events, and
- 2) they do not capture water stress of crops in the short-term (changes in the VI dynamics account at time windows of 1-2 weeks) (Nagler et al., 2013).

However, in irrigated agrosystems at arid and semiarid regions, the total of rainfall water effectively lost by evaporation is commonly considered negligible in comparison with total transpiration (first limitation). The second limitation is less of an issue when it can be assumed that the irrigation practices do not change significantly over short time periods, or in case the methods is used for the analysis with timesteps of more than 1 week to 1 month – as vegetation generally responds in that timeframe to water stress which is then captured by the satellite.

Due to favorable water availability conditions, irrigated agrosystems can be considered similar to riparian and groundwater dependent ecosystems in terms of water balance (Eamus et al., 2015). From Bowen and eddy covariance measurements of actual evapotranspiration taken in



the semiarid San Pedro and Middle Rio Grande rivers, Nagler et al. (2005) suggested the generalized relationship for estimating actual evapotranspiration

$$ET_a = ET_0 \cdot [a(1 - e^{(-bEVI)}) - c]$$

Equation 2

in which $(1 - e^{(-bEVI)})$ is a derived-function of the Beer-Lambert Law which assumes a linear relationship between EVI (*Enhanced Vegetation Index*) and LAI for values in the 0-4 m²/m² - range. Parameters a, b and c are coefficients that should be calibrated by regression analysis with local data. Values of 1.65, 2.25 and 0.169 were found by Nagler et al. (Nagler et al., 2013) for predicting ET_a in phreatophytic and irrigated crop systems in the semiarid USA taken ET₀ as the reference evapotranspiration computed following the FAO-Penman-Monteith formulation (E_{ref}). According to Equation 2 and the Nagler's parameterization, the ET_a/ET_{ref} ratio (known as the actual crop coefficient or K_c if crops are considered) would reach a maximum value of 1.28. The maximum K_c observed by Nagler et al.'s in their study was close to 1.6. Despite Nagler's approach is widely used, the empirical K_c threshold derived from its parameterization is lower than maximum daily values of crop coefficients reported in literature.

Some authors have used other satellite data, besides VIs, as land surface temperature (LST) to increase the predictive power of the ET methods. LST, or the LST-T_a difference, is a key parameter in SEB methods. However the use of these variables as direct predictors of ET_a is still limited: only few studies have used LST in empirical relationships for this purpose (Wang et al., 2006). Also, in arid and semiarid regions, LST has been found to be a good proxy of the radiative and advective forcings of evapotranspiration and, consequently, of potential evapotranspiration or ET₀ (Cammalleri and Ciraolo, 2013; Maeda et al., 2011).

The first part of this analysis aims to test the feasibility of developing an empirical relationship to compute daily evapotranspiration rates in Citrus orchards using satellite data. The key question is to which degree it is possible to get a generic functional relationship to quantify evapotranspiration from only satellite-based data, independent of local meteorological measurements. This could potentially open the way to an operational application to quantify water and energy balances in irrigated Citrus orchards.

1.3 Primary production models

The significant influence of land use and agriculture on the global carbon balance and thus the possible climate change has been recognized by many authors over the last decades. Net primary production (NPP) is a key component of the global carbon cycle. Nevertheless there are notable problems associated with field-measurement techniques for NPP. Destructive methods are required to directly estimate the NPP for a given period of accumulation, but even these have their limitations and rarely give a complete account of the net carbon flux. But most importantly, they only provide point-estimates and thus models need to be used to aggregate these numbers at the regional or global scale.

Following Cramer et al. (Cramer et al., 1999) and Ruimy et al. (Ruimy et al., 1999), two major groups of models can be distinguished:

A) Diagnostic models (also known as Production Efficiency Models -PEMs- or *satellite-based* models).

These models are based on the theory of light use efficiency (LUE) (Monteith and Moss, 1977) which states that a relatively constant relationship exists between photosynthetic carbon uptake and radiation receipt at the canopy level (McCallum et al., 2009). They are usually used for global scales, and take satellite-based data as main inputs. In general, the fraction of solar radiation absorbed by vegetation (FPAR) is estimated from indices of vegetation greenness (e.g. NDVI, EVI, SAVI) or chlorophyll content (e.g. PRI). The conversion of the absorbed PAR by vegetation into dry matter is computed using a maximum Light Use Efficiency parameter (LUE_{max}) which is scaled by one or several environmental stressors.

Depending on the requirements of auxiliary meteorological data to compute the carbon balance, PEMs can be grouped into:

A.1) LUE_{max} -constant models (e.g. CASA, SDBM, TURC, C-Fix). Because LUE changes depending on the plant functional type and the phenology, these type of models are not advised at all (McCallum et al., 2009)

A.2.) LUE_{max} -derived models (e.g. GLO-PEM, MOD17, BEAMS, EC-LUE, VPM). These models adopt different LUE values depending on the vegetation type.

A.3.) Empirical-based models (e.g. TG, GR, VI, MOD-PCM). These models assume simplified versions of Eq. (1) based on the relationships between remote sensing data and key factors affecting photosynthesis.

Models integrated in A.1. and A.2. requires ground meteorological observations as input variables. Because these observations usually have insufficiently detailed temporal and spatial resolution, errors may emerge in simulating the carbon balance (Gao et al., 2014). Models in the A.3. category reduce or avoid their dependence on ground meteorological observations, but the ecological meaning of the model parameters is not as clear as in A.1. and A.2. models (Yang et al., 2013).

B) Mechanistic models (also known Canopy Photosynthesis Models, CPMs).

Two sub-groups are distinguished (Bonan, 2008)

B.1.) Models that simulate carbon fluxes using a prescribed vegetation structure (e.g. BIOME-BGC, CARAIB, CENTURY, FBM, HRBM, KGBM, PLAI, SILVAN and TEM)

B.2.) Models that simulate both the carbon fluxes and the temporal dynamics of community composition and transitions between different plant functional types (BIOME3, DOLY, HYBRID, PnNet, 3-PG, MAPSS, FORSKA, LPJ). In these models carbon is typically represented as aggregate pools of leaf, stem, and root biomass or as an “average” plant type and density (Bonan, 2008)

Different intercomparison exercises have been developed in the last years. Probably the most extensive effort was realized during the Postdam'95 intercomparison project (Cramer and Field, 1999) in which 17 biogeochemical and biogeographical models, including PEMs, were considered (**Error! Reference source not found.**). A set of relevant papers derived from this project were collected in a special issue (Volume 5, Issue S1) published in *Global Change Biology* in 1999. The key messages from this intercomparison were collected by (Cramer et al., 1999), i.e.:

- Broad global patterns of NPP and the relationship of annual NPP to the major climatic variables agreed in most areas. Observed differences could not be attributed to the



fundamental modelling strategies, with the exception that nutrient constraints generally produced lower NPP.

- Regional and global NPP were sensitive to the simulation method for the water balance (Churkina et al., 1999).
- Seasonal variation among models was high, both globally and locally, suggesting the existence of specific deficiencies in some of the models tested.

2 Data and methods

2.1 Study area

The study area is located at Campo de Cartagena basin at SE of Spain. In these area, three eddy-covariance systems were installed and measuring micrometeorological variables during the 2009-2014 period. Eddy towers were located at commercial farms located at Villa Antonia, Casa Mulero and Casa Galindo (Figure 1 and Table 1). For the purposes of this analysis only Villa Antonia and Casa Mulero were included as calibration stations. Casa Galindo was excluded.

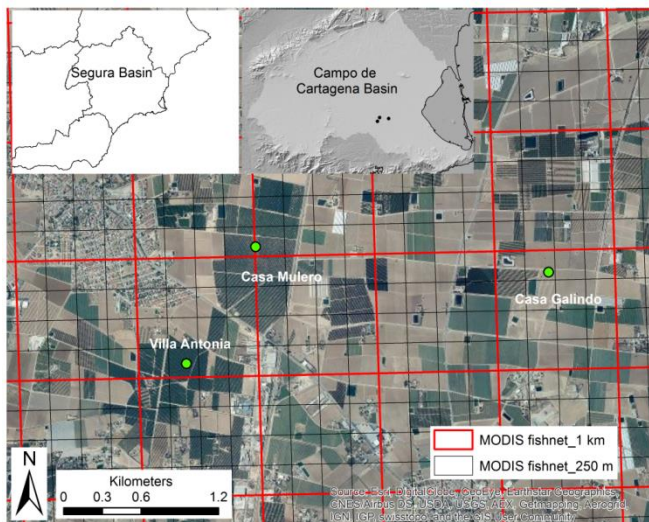


Figure 1. Study area.

Table 1. EC systems at the study area

EC Station	LONG, LAT (WGS84)	XUTM, YUTM (ETRS89)	Measurement period
Villa Antonia	-0.986, 37.701 ^a	677563, 4174550	Jul/2009 – Jan/2014
Casa Mulero	-0.979, 37.709	678099, 4175450	Aug/2009 – Jul/2011
Casa Galindo	-0.954, 37.707	680371, 4175250	Dec/2011 – Aug/2014

^a 0° 59' 9.6", 37° 42' 3.6"

2.2 Satellite data products

The vegetation index products from the MODIS sensors on Aqua (MYD13Q1) and Terra (MOD13Q1) satellite platforms were retrieved for both experimental stations from the USGS ftp server (Table 2). Terra and Aqua overpass times are around 1030 and 1330 local solar time in



its ascending (daytime) mode and 2230 and 0130 in its descending (nighttime) mode respectively. Timeseries of VIs (NDVI and EVI) at day and night were generated through a python script specifically developed in the frame of this project. Both VI products consists of 16-days Maximum Value Composite (MVC) maps at 250 m of spatial resolution (23 scenes per year), but with time-window centroids moved 8-days each other. Before their processing, values for both timeseries were filtered according the MODIS-quality flags which are included for each MODIS product.

After excluding values with low reliability, MOD13Q1 and MYD13Q1 were composited to retrieved 8-day timeseries (Figure 2). The resulting timeseries were finally filtered using local polynomial functions based on an adaptive Savitzky-Golay filter. Filtering of satellite-based VIs is a critical and widely used practice to remove spike and spurious values, to fill gap values, and to extract the downward trend typically observed in the vegetation indices as consequence of atmospheric effects (Chen et al., 2004; Jönsson and Eklundh, 2002). The Savitzky-Golay post-filtering of VI fields was done using the TIMESAT software (Jönsson and Eklundh, 2004). A time-window of 5 consecutive MVCs, a double iteration to the upper envelope, and an adaptive strength of 2 in a scale from 1-12 was used.

Additionally to the 16-day composites VI timeseries, daily values of Land Surface Temperature (day and night values) (MYD11A1 and MOD11A1 products), and Black-sky albedo (MCD43B3) were also retrieved for both EC stations. Values with low reliability according the quality data layer within each product were rejected from the analysis. Daily values were also averaged at the 8-day level.

Table 2. Satellite-based variables used in this study

Variable	MODIS product	Spatial Res.	Temporal Res.
Vegetation Index (NDVI, EVI)	MOD13Q1 (Terra)	250-m	16-d
	MYD13Q1 (Aqua)	250-m	16-d
Land Surface Temperature	MOD11A1 (Terra)	1-km	1-d
	MYD11A1 (Aqua)*	1-km	1-d
Albedo	MCD43B3	1-km	1-d
	(Terra+Aqua)		

* All LST data analyzed and shown in this report refer to LST day from Aqua (LST_{a,d})

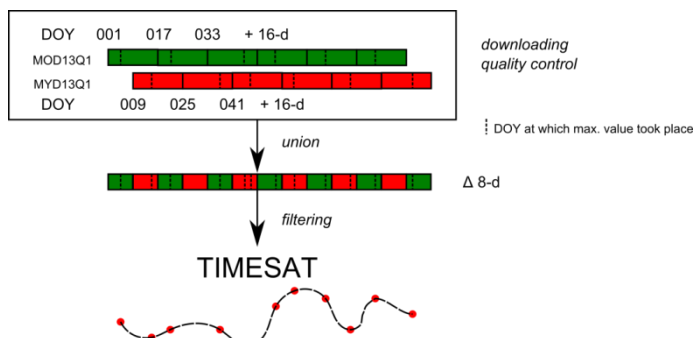


Figure 2. Retrieval of 8-day timeseries from 16-d composite values of vegetation indices.

2.3 Ground-based energy and water balance measurements

VA and CM experimental sites were equipped with EC systems for measuring λE and H fluxes using a three-dimensional sonic anemometer of high-frequency (CSAT-3, Campbell Scientific, Logan, UT, USA) and an IRGA (open-path infrared gas analyzer, LICOR Li-7500, Campbell Scientific, USA). Both devices, the CSAT-3 and Li-7500, were installed at VA, CM at 1.5 m (Martin-Gorriz et al., 2011). All sensors sampled at 10 Hz and fluxes were estimated and stored half-hourly applying standard corrections for axis-rotation and density fluctuations.

Incoming solar radiation at VA and CM was measured with a pyranometer (CMP3, Kipp & Zonnen, Delft, The Netherlands). Soil heat flux was measured by means of two heat flux plates (REBS, model HFT-3.1, Seattle, WA, USA) buried 5 mm below the surface, near a dripper (wet bulb) and in the middle of the row (dry soil), respectively. T_a and relative humidity (RH%) were measured with thermohygrometers.

Energy closure in EC systems is usually not reached because of systematic bias in instrumentation, mismatch in source areas, neglected energy sinks, problems of scalar similarity, or landscape heterogeneity (Foken, 2008; Wilson et al., 2002). When available energy is known and error in its measurement is moderate, forcing the energy balance closure is widely justified. In this study, energy balance closure was forced at the daily scale using the Bowen-ratio method (Twine et al., 2000). Before the analysis, potential outliers (days with Bowen ratios (H/LE) less than -0.75 (Xing et al., 2008), and crop coefficients higher than 2.5) were identified and excluded (Figure 3). Daily values were finally averaged and scaled up to 8-days temporal windows compatible with the satellite-based composite MODIS VI-LST products (see section 2.2).

Daily crop-coefficients were computed as the ratio between measurements of actual evapotranspiration (LE) and potential evapotranspiration (ET_0). Here, ET_0 was computed through by three ways using the, the FAO56 Penman-Monteith equation (reference evapotranspiration, E_{ref}) (Allen et al., 1998). Other methods to quantify ET_0 , i.e. the Priestley-Taylor equation (E_{eq} , Equation 4) (Priestley and Taylor, 1972) and the Makkink equation (E_{mak} , Equation 5) (Makkink, 1957), have been computed and delivered in the dataset but are not refereed in this report. At the 8-day level, the Hargreaves-Samani potential evapotranspiration (E_{HS} , Equation 6) (Hargreaves and Samani, 1985) was additionally computed and analyzed as a potential predictor of the energy/water balance at the 8-day level.

$$E_{ref} = \frac{s \cdot (R_n - G) + \gamma \cdot \frac{900}{T_a} \cdot u_2 \cdot VPD_a}{s + \gamma(1 + 0.34 \cdot u_2)}$$

Equation 3

$$E_{eq} = \frac{s}{s + \gamma} \frac{R_n - G}{\lambda}$$

Equation 4

$$E_{mak} = \frac{s}{s + \gamma} \left(0.61 \frac{R_s}{\lambda} - 0.12 \right)$$

Equation 5

$$E_{HS} = a \cdot R_a \cdot (T_{avg} + b) \cdot (T_{max} - T_{min})^{0.5}$$

Equation 6

where s is the slope of vapour pressure curve (kPa/°C), γ is the psychrometric constant (kPa/°C), R_a , R_s and R_n are the extraterrestrial, incoming and net radiation respectively



(MJ/m².day), VPD is the vapour pressure deficit of the air (kPa), u_2 is the wind speed at 2 m (m/s), and λ the latent heat of vaporization (MJ/kg). T_a in Equation 3 is the temperature of the air (°C), while T_{avg} , T_{max} and T_{min} in Equation 6 are the average, maximum and minimum air temperatures recorded during the period of interest. Parameters a and b in the HS equation are calibration parameters. The best overall local fitting, including VA and CM stations, with FAO-Penman-Monteith recorded at the 8-day level was reached with $a=0.1827$ and $b=-0.3911$.

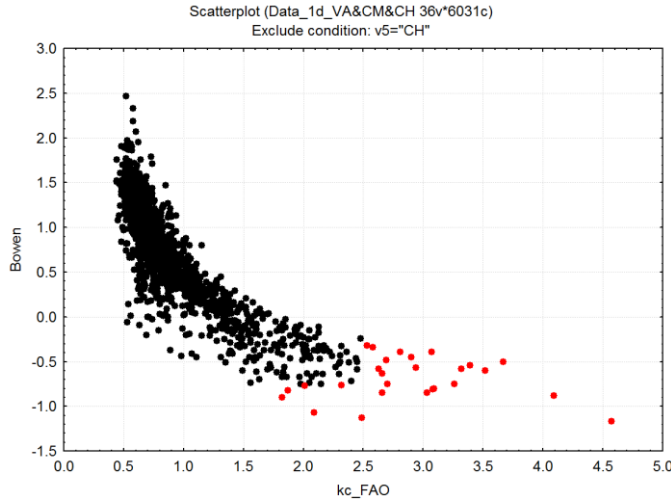


Figure 3. Outliers (red circles) excluded from the analysis.

Field-based Leaf Area Index (LAI) measurements were taken at plot scale at both sites. For this analysis, LAI was used as part of a first assessment to evaluate the confidence of satellite-based vegetation indices and the coupling of LAI with energy/water measurements. This assessment was only realized at Villa Antonia and for one-year period ranging from February-2010 to February-2011, when LAI was quarterly quantified at the field scale using ceptometer measurements (LAI-2200C, Campbell Scientific, USA).

2.4 Net primary production

As mentioned in the Introduction of this report, several reviews (e.g. McCallum et al. (2009)) and intercomparison exercises (e.g. Huntzinger et al. (2012)) have been provided over the last years on satellite-based terrestrial Production Efficiency Modeling (PEM). Many of these models use the Light Use Efficiency principle, so gross and net primary production are usually computed as follows:

$$GPP = PAR * FPAR * LUE_{max} * f \quad [Eq. 1]$$

and

$$NPP = GPP - (MR_a + GR_a) \quad [Eq.2]$$

in which GPP, NPP = Gross or Net Primary Production, respectively (gC/m²); PAR = Photosynthetically Active Radiation (MJ/m²); FPAR = Fraction of Absorbed PAR by vegetation/canopy(dimensionless); LUE_{max} = maximum (unstressed) Light Use Efficiency (gC/MJ); f = scalar value [0-1] which reduces the maximum LUE due to physiological or

environmental stress conditions (dimensionless) and MR_a , GR_a = maintenance and growth autotrophic respiration (gC/m^2).

In general, PAR is computed as $0.45 \cdot R_s$, being R_s the shortwave incoming radiation (MJ/m^2). FPAR is a parameter difficult to measure directly, so is usually inferred from models describing the transfer of solar radiation in plant canopies using remote sensing observations as constraints (McCallum et al., 2009).

In general, there are two common ways to quantify FPAR, i.e.

a) using a Beer-Lambert law relationship with LAI, and the following equation:

$$FPAR = 0.95 * [1 - \exp(-k * LAI)] \quad [Eq. 3]$$

being LAI the Leaf Area Index (leaf area per ground area, m^2/m^2), and k the light extinction coefficient (dimensionless) which takes values from 0.3 or less in canopies with linear, vertical leaves, to 1.0 or more in canopies with flat, horizontal leaves (Campbell, 1986). A constant value of 0.5 is commonly used in PEMs.

b) using a linear relationship with a satellite-based vegetation index (Asrar et al., 1992; Gamon and Qiu, 1999; Hatfield et al., 1984; Wiegand et al., 1991).

Recently, Ogutu and Dash (2013a) proposed an alternative way for deriving FPAR values from ground-based measurements of Net Ecosystem Exchange and PAR.

According [Eq.2], NPP is computed as the difference between the GPP and the autotrophic respiration (R_a) which is diverted into the respiration invested for maintenance purposes (MR_a) and for growth (GR_a).

An overview of 13 PEMs is provided in Appendix I. Most of these models have been widely used in research, being the most cited the CASA model followed by the GLO-PEM and the operational MOD17 model (Figure 4).

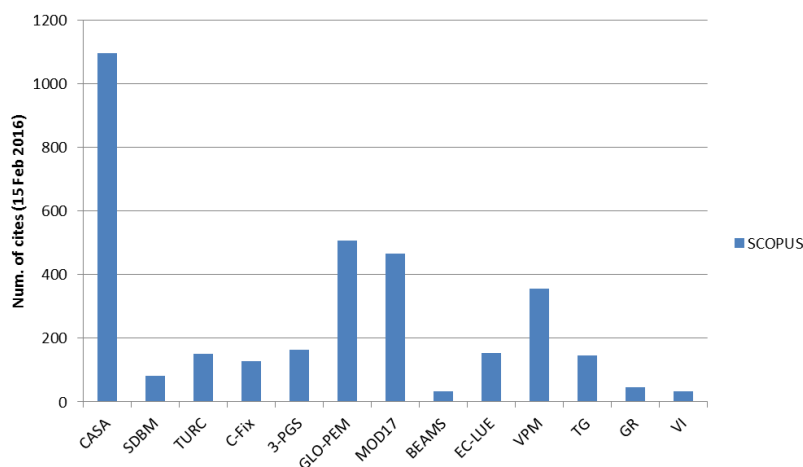


Figure 4. Number of cites registered until 15-Feb-2016 in SCOPUS for each PEM-Diagnostic model.



According to a recent study developed by Chen et al. (Chen et al., 2011), LUE_{max} estimates vary by at least a factor of 2. They used 12 agricultural eddy-flux measurement sites in North America and Europe to constrain LUE models in general and LUE_{max} in particular, and found that LUE models could explain on average about 70% of the variability in net ecosystem exchange (NEE) when LUE_{max} was increased from 0.5 to 0.65–2.0 gC/MJ. Chen et al.'s results imply that croplands are more important in the global carbon budget than often thought, suggesting that inverse modeling approaches that utilize LUE model outputs as a-priori input should be revisited in areas where croplands are an important contributor to regional carbon fluxes. These authors do not advise the use of constant LUE_{max} values, and highlight the importance of accurate land surface parameterizations to achieve reliable carbon monitoring capabilities from remote sensing information.

Table 3. PEM models reviewed.

Group	Sub-group	Acronym (n. of cites)	Full name	GPP/NPP estimated as	LUE _{max} (gC·m ⁻² ·MJ ⁻¹)	Scalars	Time resolution	Key reference	Others	
Diagnostic models (also known as Production Efficiency Models, PEM) <i>Satell</i>	LUE _{max} constant	CASA	Carnegie Ames Standford Approach	NPP (direct)	0.39	T, SM	Monthly	(Potter, 1993)		
		SDBM	Simple Diagnostic Biosphere Model	NPP = PAR * FPAR(NDVI) * LUE _{max} * Sc NEP = NPP - Rh(Tair,Alpha)	1.00	ET/ET _{eq}	Monthly	(Knorr and Heimann, 1995)		
		TURC	Terrestrial Uptake and Realease of Carbon	NPP=GPP-Ra	1.10				(Ruimy et al., 1996)	
		C-Fix		NPP=GPP-Ra	1.10	T, SM, CO ₂	Daily	(Veroustraete et al., 2002)	Pre-Operational	
		3-PGS		GPP; NPP=0.45*GPP	1.80	Frost days, SM, VPD	Monthly	(Coops et al., 1998)	Forests	
LUE _{max}	GLO-PEM	Global Production Efficiency Model	NPP=GPP-Ra	C3: 55.2*Alpha C4: 2.76	T, SM, VPD		(Goetz et al., 1999; Prince, 1991; Prince and Goward, 1995)			



Group	Subgroup	Acronym (n. of cites)	Full name	GPP/NPP estimated as	LUE _{max} (gC·m ⁻² ·MJ ⁻¹)	Scalars	Time resolution	Key reference	Others
ite-based	derived	MOD17		NPP=GPP-Ra=GPP-MR-GR*	0.997 - 1.382 (based on MODIS biome)	Tmin, VPD	Daily: GPP, Leaf_MR, Froot_MR, PSNnet Yearly: Lwood_MR, GR, NPP	(Heinsch et al., 2006; Running and Zhao, 2015)	Operational
		BEAMS	Biosphere	NPP=GPP-RA		P/Pmax=f(T, RH, SM, CO2)	Monthly	(Sasai et al., 2005)	
		EC-LUE	Eddy Covariance Light Use Efficiency Model		2.14 (for forests, grasslands, savannas)			(Yuan et al., 2007)	
		VPM	Vegetation Photosynthesis Model	GPP	evergreen needle-leaf forests: 2.208 tropical evergreen forests: 2.484	T, W, Leaf phenology (LSWI)		(Xiao et al., 2004)	

Group	Subgroup	Acronym (n. of cites)	Full name	GPP/NPP estimated as	LUE_{max} ($gC \cdot m^{-2} \cdot MJ^{-1}$)	Scalars	Time resolution	Key reference	Others
	Empirical VI-based models	TG	Temperature and Greenness Model	$GPP = m(LST) * (LST_{sc} * EVI_{sc})$				(Sims et al., 2008)	
		GR	Greenness and Radiation Model	$GPP = VI_{chl}(VI) * PAR$				(Gitelson et al., 2006)	
		VI	Vegetation Index Model	$GPP = PAR * FPAR(VI) * LUE(VI)$				(Wu et al., 2010c)	
		TGR	Temperature and Greenness Rectangle					(Yang et al., 2013)	
		MOD-PCM	MODIS-based Photosynthetic Capacity Model	$GPP = PC_{max} * EVI * W$		$W = f(LSWI)$	8-day	(Gao et al., 2014)	



Table 4. Comparison and performance analyses found in literature for Production Efficiency Models.

References	(Cramer et al., 1999)	(McCallum et al., 2009)*	(Wu et al., 2010a)	(Wang et al., 2011)**	(Tan et al., 2012)*	(Kelley et al., 2013)***	(Ogutu and Dash, 2013b)	(Yang et al., 2013)	(Gao et al., 2014)	(Liu et al., 2014)	(Dong et al., 2015)
Biomes	Global	--	USA DBF	Global Benchmarking assessment	CRP (tropical palm plantations)	Global Benchmarking assessment	USA ENF[2], DBF[2], SAV, GSS CRP[2] (corn, soybean/corn)	USA ENF[7], EBF[2], DBF[7], MXF[3], SAV[2], SHR[2], GSS[4] CRP[3] (corn/soybean, maize, maize- soybean)	China MBF, tSTE, mSTE, aSHR, aMAR	China EBF[2], ENF, MXF, GSS[3] CRP[1] (wheat/corn)	USA GSS (tallgrass prairie) CRP[2] (soybean, maize)
CASA	x	x		x	x		x				
SDBM	x					x					
TURC	x	x			x						
C-Fix		x			x		x				
3-PGS					x						
GLO-PEM	x	x			x						
MOD17		x	x		x		x		x	x	
BEAMS		x									
EC-LUE					x						
VPM			x		x				x	x	x
TG			x		x			x		x	x
GR								x		x	x
VI			x		x					x	x
TGR								x			
MOD-PCM									x		

Biomes: ENF = Evergreen Needleleaf Forest, EBF = Evergreen Broadleaf Forest, DBF = Deciduous Broadleaf Forest, MBF = Mixed Broadleaf Forest, MXF = Mixed Forest, SAV = Savanna, SHR = Shrubland, STE = Steppe, GSS = Grassland, CRP = Crop. Prefixes: t = temperate, m = meadow, a = alpine

* Not a intercomparison assessment s.s.

** Models used: CASA, BIOME-BGC, LPJ, TOPS-BGC.

*** Models used: SDBM, LPJ, LPX.

3 Results and discussion

3.1 Analysis of field data

Field-based LAI values at Villa Antonia ranged between 3.0 and 4.0 m^2/m^2 . From the end of April-2010 just before the pruning at the second week of October, LAI remained in the 3.6 and 4.0 range. Because trees were pruned in the second week of October-2010, LAI dropped off by 23% up to values of 3.0 and, since then increased slightly up to reach 3.4 at the beginning of March-2011.

In general, LAI measurements tracked well actual evapotranspiration measurements ($R^2=0.70$) (Figure 5). None of the satellite-based vegetation indices analyzed, EVI and NDVI, did track the LAI dynamics (Figure 7). EVI was better, but still very weakly, correlated with LAI measurements than NDVI which showed an opposite dynamics and a negative correlation.

Because of the lack of coupling between LAI and vegetation indices, which may be associated with the low spatial resolution of MODIS-VI products (250 m) for highly heterogeneous landscapes, it is expected that none of the satellite-based variables can explain the energy fluxes accurately. Among the satellite-based variables, land surface temperature at midday (LST_d) was by far the best predictor in explaining actual evapotranspiration ($R^2=0.88$, Figure 7)

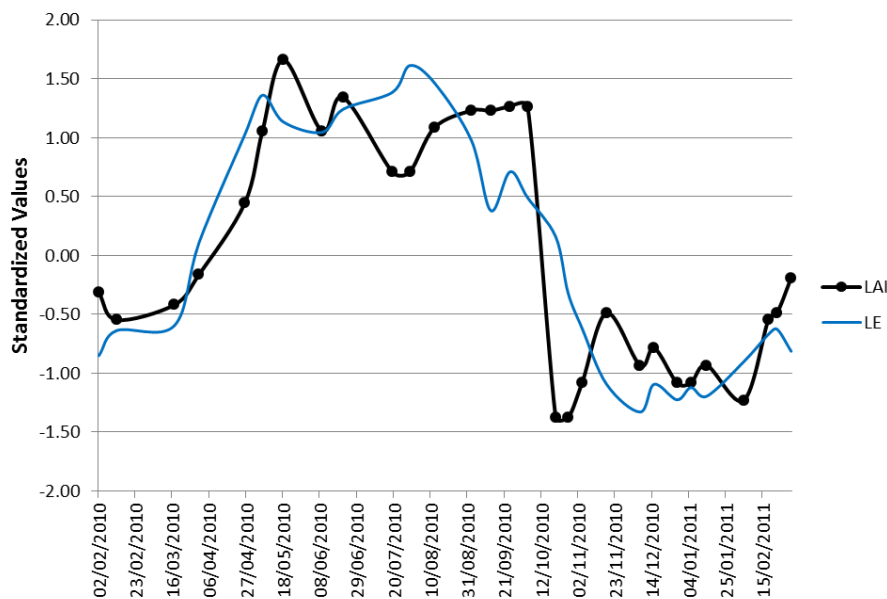


Figure 5. Standardized trajectories of field-based LAI measurements, and actual evapotranspiration (LE) and Gross Primary Production (GPP) observed at Villa Antonia from February-2010 to February-2011.

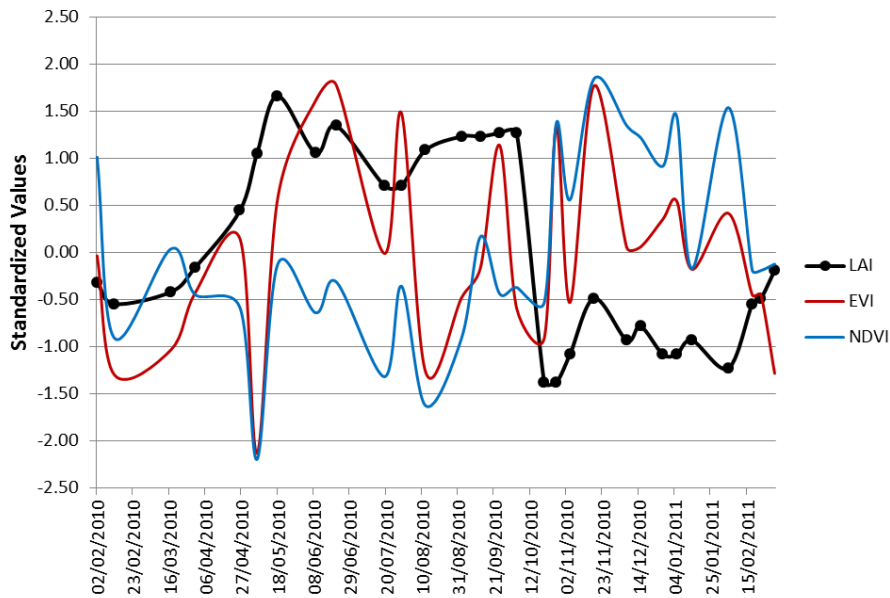


Figure 6. Standardized trajectories of field-based LAI measurements, and satellite-based vegetation indices (EVI and NDVI) observed at Villa Antonia from February-2010 to February-2011.

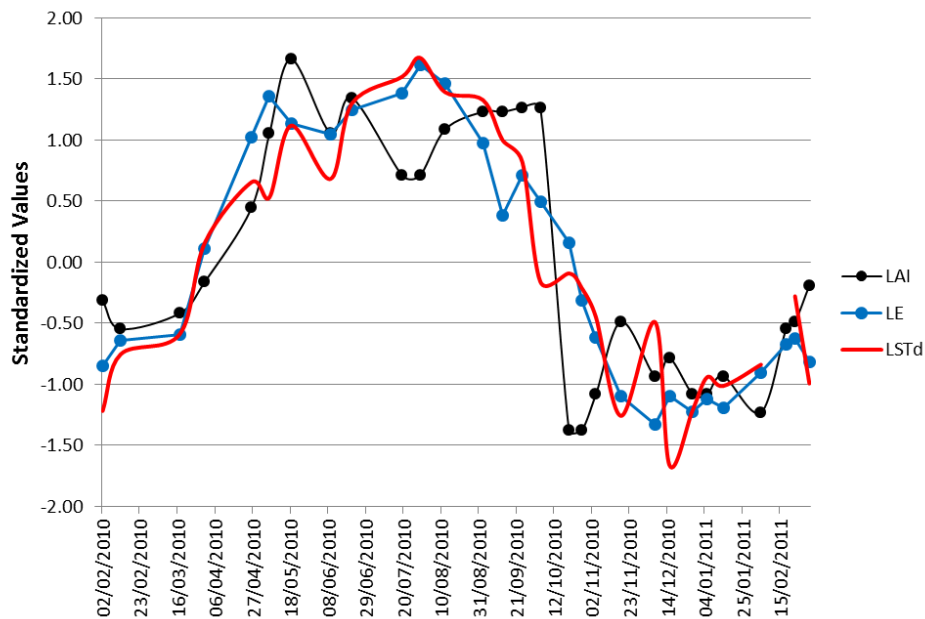


Figure 7. Standardized trajectories of field-based LAI measurements, actual evapotranspiration (LE) and satellite-based Land Surface Temperature at midday (LST_d) observed at Villa Antonia from February-2010 to February-2011.

3.2 Energy and crop-coefficient dynamics

Daily and 8-day trajectories of turbulent energy fluxes (latent and sensible), evaporative fractions and crop coefficients for Villa Antonia and Casa Mulero sites are shown in Figure 8 and Figure 9, respectively.



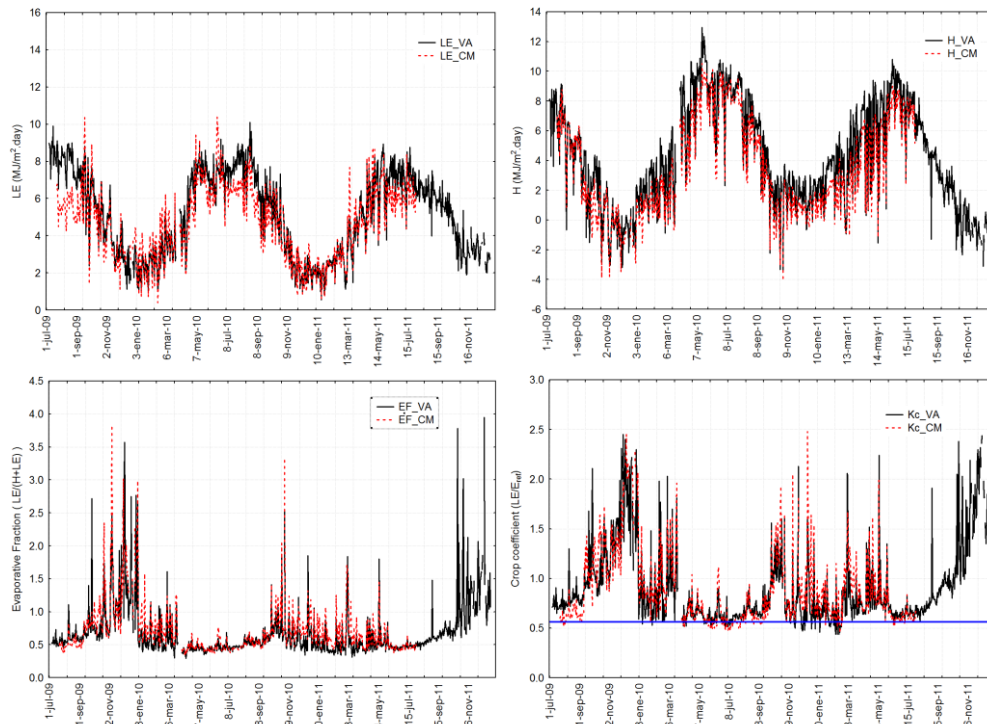


Figure 8. Daily turbulent fluxes (upper-left: latent heat, upper-right: sensible heat), and evaporative (lower-left) and crop coefficient (lower-right) values measured in experimental stations. Solid-black: Villa Antonia (VA); dashed-red: Casa Mulero (CM); blue line in lower-right panel defines the basal crop coefficient adopted for both systems.

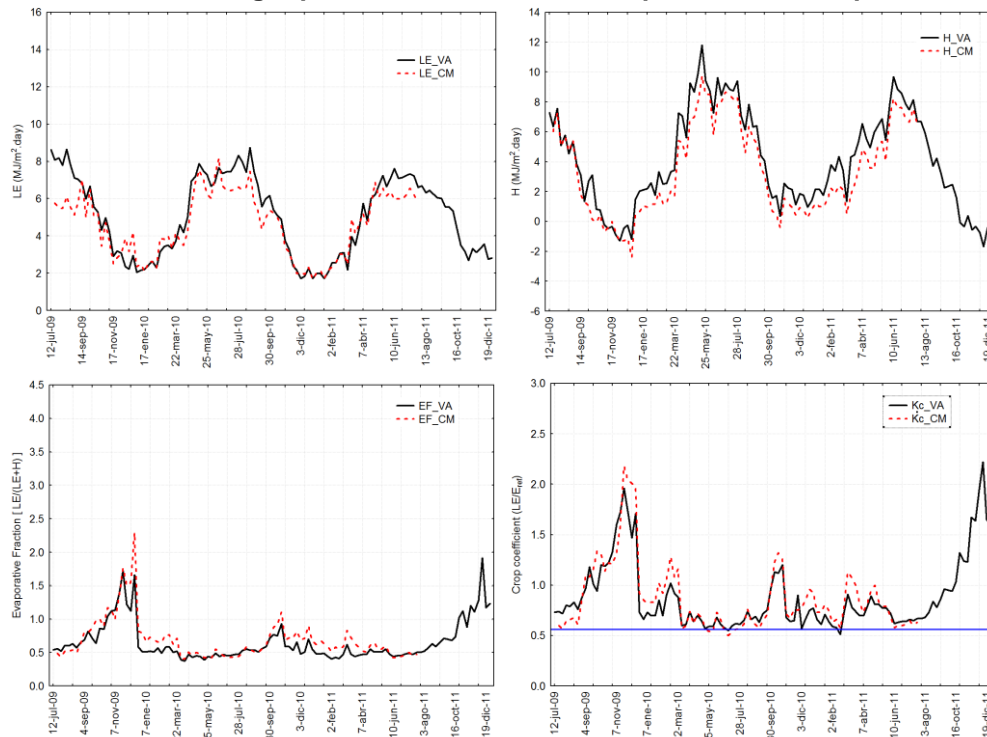


Figure 9. 8-day averaged turbulent fluxes (upper-left: latent heat, upper-right: sensible heat), and evaporative (lower-left) and crop coefficient (lower-right) values measured in experimental stations. Solid-black: Villa Antonia (VA); dashed-red: Casa Mulero (CM); blue line in lower-right panel defines the basal crop coefficient adopted for both systems.



During the common period with data in both VA and CM experimental stations, i.e from beginning of July-2009 to end of July-2011, significant statistical differences in turbulent fluxes, energy ratios and crop coefficient were observed (Table 5).

Table 5. Average \pm standard errors of turbulent fluxes (LE=latent; H=sensible), Bowen ratio (H/LE), evaporative fraction (LE/(H+LE)) and crop coefficient (LE/E_{ref}). Statistics refer to the common measuring period. Statistical differences (*)=p-level<0.01) was detected using a t-test for dependent samples.**

Variable	VA	CM	Statistical difference
LE	5.18 \pm 2.33	4.70 \pm 1.94	***
H	4.60 \pm 3.46	3.53 \pm 3.25	***
Bowen ratio (β)	0.85 \pm 0.53	0.68 \pm 0.53	***
Evaporative fraction (EF)	0.62 \pm 0.33	0.70 \pm 0.38	***
Crop coeff. (k _c)	0.83 \pm 0.33	0.87 \pm 0.36	***

For the combined pool of data from VA and CM, negative Bowen values were concentrated during the autumn and winter seasons (Figure 10) while the highest evapotranspiration rates with median values of 7 MJ/m².day (81 W/m² or 2.85 mm/day) were observed during the end of spring (May) to the end of summer (August) (Figure 11). On average, during these months the evaporative fraction accounted almost 50% of the total available energy, while evapotranspiration accounted between 45% (CM) and 50% (VA) of the total mean annual evapotranspiration.

Crop coefficients values showed a higher seasonality and monthly dispersion, with median values higher than 1.0 during the October-December period when evapotranspiration usually exceeds the reference evapotranspiration. During the rest of the year which includes the most critical growing period, crop coefficient values ranged between 0.6 and 0.8, which is in agreement with the values reported for *Citrus* by FAO and other studies (Petillo and Castel, 2007). A basal crop coefficient (K_{cb}) of 0.56 has been stated as a representative value for both sites (Figure 8 and Figure 9).

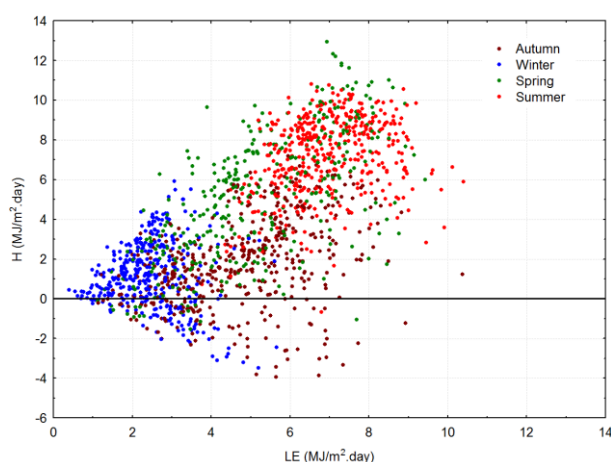


Figure 10. Sensible vs Latent heat fluxes scatterplot observed at VA and CM experimental stations.



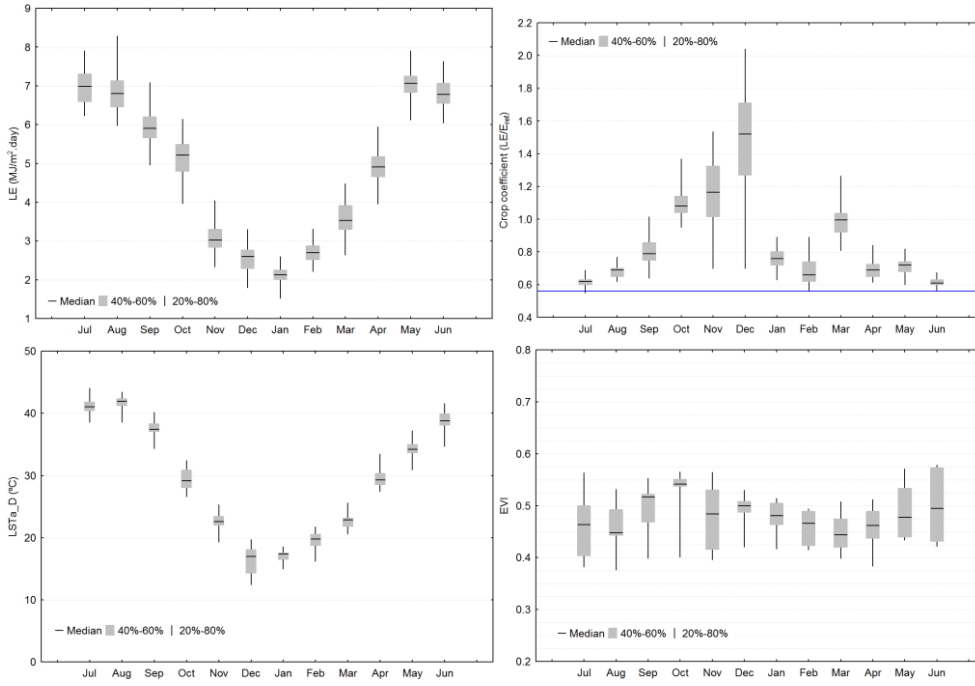


Figure 11. Monthly boxplots of daily actual evapotranspiration (LE, left) and crop coefficients (k_c , right) measured in Villa Antonia and Casa Mulero experimental stations. Percentages represents the value of percentile taken.

Slopes from the E_{ref} -LE relationship between CM and VA, a parameter which is related with the average crop coefficient, were statistically different (p -value<0.01) between sites, being 16% higher in VA than in CM (Figure 12). This difference is also observed at the 8-day level.

$$LE_{VA_1d} = 1.5882(\pm 0.0643) + 0.5257(\pm 0.0082) * E_{ref} \quad [n = 888, R2 = 0.82]$$

$$LE_{CM_1d} = 1.8275(\pm 0.0811) + 0.4549(\pm 0.0112) * E_{ref} \quad [n = 716, R2 = 0.70]$$

$$LE_{VA_8d} = 1.5733(\pm 0.1593) + 0.5278(\pm 0.0211) * E_{ref} \quad [n = 114, R2 = 0.85]$$

$$LE_{CM_8d} = 1.9472(\pm 0.1868) + 0.4372(\pm 0.0265) * E_{ref} \quad [n = 94, R2 = 0.75]$$

$$LE_{VA\&CM_1d} = 1.6714(\pm 0.0513) + 0.4989(\pm 0.0068) * E_{ref} \quad [n = 1604, R2 = 0.77]$$

$$LE_{VA\&CM_8d} = 1.7158(\pm 0.1235) + 0.4924(\pm 0.0168) * E_{ref} \quad [n = 208, R2 = 0.81]$$

Standard errors of parameters are shown between parentheses. E_{ref} is the reference evapotranspiration computed using the Penman-Monteith-FAO formulation. LE is the actual evapotranspiration. Both E_{ref} and LE in MJ/m².day



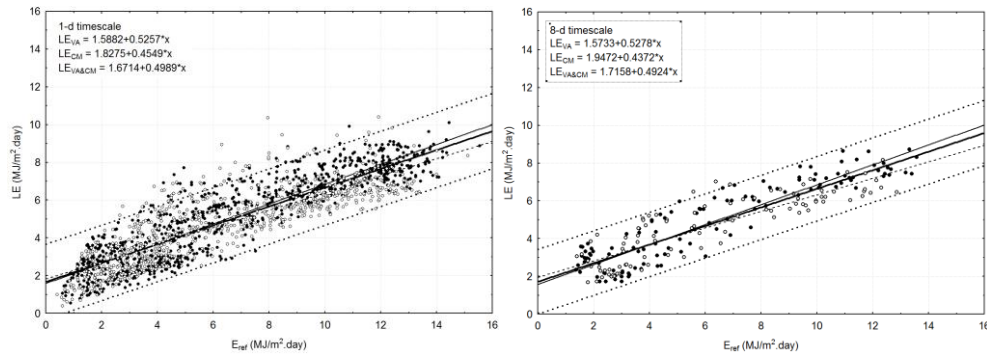


Figure 12. Slopes of the E_{ref} -LE relationship (average crop coefficient) for VA (filled circles, solid line) and CM (open circles, dashed line). Dotted line shows the 95% prediction band for the overall pool of data.

3.3 Calibration of empirical ET relationships

Pearson correlation coefficients among turbulent fluxes and energy ratios, and meteorological and satellite-based variables are shown in Table 6. When both sites were treated together, incoming solar radiation - R_g - or reference evapotranspiration (E_{ref}) were the best predictors for both latent and sensible heat fluxes. This finding is not surprising at all, as the available radiation at the surface level is the main driver of the evaporation and transpiration processes, especially in those environments in which water is not a limiting resource.

The inclusion of the advective term in the Penman-Monteith equation barely increases the predictive power of the model in comparison with a model which includes the radiative forcing driver by alone. Daily average temperature of the air measured at each site or the satellite-based land surface temperature were the second highest predictor of LE. As it occurs with R_g and E_{ref} , correlation coefficients observed between LE vs T_a or LST were strongly similar proving that that satellite or ground-based measurements can be equally used in empirical relationships. Similar results have been observed by Wang et al. (Wang et al., 2006).

As it was stated from the preliminary assessment, vegetation indices were poorly or slightly correlated with turbulent fluxes. The apparent high negative correlation between latent and sensible heat with NDVI in VA and CM is thought to be artificial. Results from Table 6 confirm the energy-limited nature of our agrosystem, in which water is always provided to fulfill the water requirements of trees.

When actual evapotranspiration is normalized regarding reference evapotranspiration (crop coefficients, k_c), air vapor pressure deficit (VPD) is the first predictor followed by land surface temperature (LST).



Table 6. Pearson correlation coefficients (r) among energy balance traits and meteorological and satellite-based data computed daily. All correlations are significant, except those with the *n.s.* flag.

Site	Var.	Meteorological				Satellite			Combined
		R _g	T _a	VPD	E _{ref}	LST _{a_D}	EVI	NDVI	LST - T _a
VA	R _n *-G	0.97	0.73	0.68	0.98	0.77	0.15	-0.77	0.66
	LE	0.90	0.83	0.70	0.91	0.86	0.16	-0.81	0.70
	H	0.91	0.57	0.58	0.90	0.60	0.12	-0.65	0.54
	Bowen	0.41	<i>n.s.</i>	0.16	0.37	<i>n.s.</i>	-0.09	-0.16	<i>n.s.</i>
	EF	-0.46	-0.10	-0.24	-0.44	<i>n.s.</i>	0.09	0.23	-0.12
	k _c	-0.46	-0.3	-0.5	-0.52	-0.19	<i>n.s.</i>	0.24	<i>n.s.</i>
CM	R _n *-G	0.97	0.75	0.69	0.97	0.81	-0.11	-0.75	0.70
	LE	0.87	0.71	0.65	0.86	0.72	-0.13	-0.73	0.60
	H	0.92	0.68	0.64	0.92	0.76	-0.08	-0.66	0.66
	Bowen	0.69	0.46	0.42	0.67	0.54	<i>n.s.</i>	-0.47	0.51
	EF	-0.67	-0.45	-0.43	-0.64	-0.54	<i>n.s.</i>	0.45	-0.50
	k _c	-0.56	-0.54	-0.63	-0.63	-0.48	<i>n.s.</i>	0.32	-0.3
VA&CM	R _n *-G	0.96	0.73	0.66	0.97	0.78	0.15	-0.41	0.68
	LE	0.87	0.77	0.65	0.89	0.79	0.15	-0.43	0.66
	H	0.90	0.61	0.58	0.91	0.67	0.14	-0.35	0.60
	Bowen	0.54	0.21	0.28	0.51	0.26	0.08	-0.14	0.28
	EF	-0.56	-0.27	-0.33	-0.54	-0.32	-0.09	0.15	-0.32
	k _c	-0.51	-0.42	-0.56	-0.57	-0.33	<i>n.s.</i>	0.18	-0.17

LE = latent heat flux (actual evapotranspiration); H = sensible heat flux; Bowen = H/LE; EF = evaporative fraction (LE/R_n*-G); K_c = crop coefficient (LE/E_{ref}, being E_{ref} the reference evapotranspiration computed according the FAO-Penman-Monteith equation)



Table 7. Pearson correlation coefficients (r) among energy balance traits and meteorological and satellite-based data computed at 8-day temporal windows. All correlations are significant, except those with the *n.s.* flag.

Site	Var.	Meteorological				Satellite		
		R _g	T _a	E _{ref}	E _{hs}	LST _{a_D}	EVI	NDVI
VA	R _n *-G	0.98	0.72	0.99	0.77	0.87	<i>n.s.</i>	-0.84
	LE	0.93	0.85	0.92	0.75	0.94	<i>n.s.</i>	-0.85
	H	0.92	0.55	0.93	0.70	0.74	<i>n.s.</i>	-0.76
	Bowen	0.51	<i>n.s.</i>	0.55	0.35	0.28	<i>n.s.</i>	-0.40
	EF	-0.51	-0.20	-0.55	-	-0.33	<i>n.s.</i>	0.42
	k _c	-0.50	-0.28	-0.57	-	-0.35	<i>n.s.</i>	0.39
CM	R _n *-G	0.98	0.63	0.98	0.78	0.88	<i>n.s.</i>	-0.79
	LE	0.90	0.71	0.87	0.76	0.86	<i>n.s.</i>	-0.83
	H	0.94	0.53	0.96	0.72	0.81	<i>n.s.</i>	-0.70
	Bowen	0.79	0.33	0.80	0.56	0.66	<i>n.s.</i>	-0.55
	EF	-0.73	-0.30	-0.74	-	-0.60	<i>n.s.</i>	0.48
	k _c	-0.59	-0.31	-0.67	-	-0.49	<i>n.s.</i>	0.32
VA&CM	R _n *-G	0.97	0.67	0.98	0.75	0.87	0.15	-0.48
	LE	0.91	0.78	0.90	0.73	0.90	<i>n.s.</i>	-0.49
	H	0.92	0.53	0.94	0.69	0.77	<i>n.s.</i>	-0.42
	Bowen	0.63	0.20	0.66	0.43	0.45	<i>n.s.</i>	-0.25
	EF	-0.60	-0.24	-0.63	-	-0.45	<i>n.s.</i>	0.25
	k _c	-0.53	-0.29	-0.61	-	-0.41	<i>n.s.</i>	0.27

LE = latent heat flux (actual evapotranspiration); H = sensible heat flux; Bowen = H/LE; EF = evaporative fraction (LE/R_n*-G); K_c = crop coefficient (LE/E_{ref}, being E_{ref} the reference evapotranspiration computed according the FAO-Penman-Monteith equation)
E_{hs} = Potential evapotranspiration according locally-calibrated Hargreaves-Samani equation.

Reference evapotranspiration on itself explained 77% (RMSE=12 W/m², relative error = 21%) of the variance observed in daily actual evapotranspiration, while land surface temperature explained 63% (RMSE=14 W/m², relative error = 22%). When both variables were included into a MLR model, the predictive power of the model increased up to explain 78% of the total variance, and the relative error was reduced by 25% (Table 8). The relative error accounted was higher during the winter months and much lower during the end of spring and summer (Figure 13).

At the 8-day level, errors were even reduced in comparison with those errors reported at the daily level. In general, the overall relative RMSE values reported in this study are in the same order of those reported in literature which indicate errors in the 10-20% range for actual evapotranspiration (Glenn et al., 2010; Wang et al., 2006). By opposite, satellite-based vegetation indices did not contribute significantly to explain actual evapotranspiration.



Table 8. Predictive error parameters reported for the LE, and E_{ref} and $LST_{a,D}$ relationships.

$LE_{VA\&CM}$	$f(E_{ref})$		$f(LST_{a,D})$		$f(E_{ref}, LST_{a,D})$	
	1-d	8-d	1-d	8-d	1-d	8-d
R^2	0.77	0.75	0.63	0.80	0.78	
MAE (MJ/m ² .day)	0.82	0.71	0.97	0.71	0.74	
RMSE (MJ/m ² .day)	1.02	0.88	1.22	0.88	0.94	
rRMSE (%)	20.58	17.91	21.60	17.93	16.25	

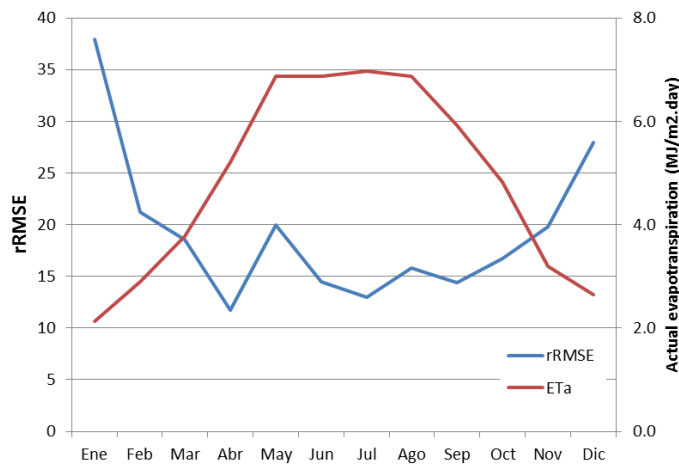


Figure 13. Monthly variation of the relative RMSE (left-axis) between observed (right-axis) and predicted values of actual evapotranspiration.

As stated before, $LST_{a,D}$ is highly correlated with LE at Villa Antonia and moderately at Casa Mulero. Linear relationships between actual evapotranspiration and land surface temperature in Villa-Antonia and Casa-Mulero are shown below and in Figure 14.

$$LE_{VA_{1d}} = -0.1372(\pm 0.1722) + 0.1903(\pm 0.0519) * LST_{a,D} \quad [n = 460, R^2 = 0.75]$$

$$LE_{CM_{1d}} = 1.2904(\pm 0.2182) + 0.1302(\pm 0.0067) * LST_{a,D} \quad [n = 374, R^2 = 0.50]$$

Despite slopes found in both sites were significantly different at the 95% level (p -level < 0.05) (<http://www.danielsoper.com/statcalc3/calc.aspx?id=103>), an overall-combined $LST_{a,D}$ -LE equation for both sites was also retrieved.

$$LE_{VA\&CM_{1d}} = 0.5141(\pm 0.1433) + 0.1634(\pm 0.0044) * LST_d \quad [n = 834, R^2 = 0.63]$$

$$LE_{VA\&CM_{8d}} = 0.1832(\pm 0.0065) - 0.4072(\pm 0.1971) * LST_d \quad [n = 204, R^2 = 0.80]$$

Standard errors of parameters are shown between parentheses. $LST_{a,D}$ is the day land surface temperature, in Celsius degrees, measured by the Aqua-MODIS sensor. LE is the actual evapotranspiration in MJ/m².day



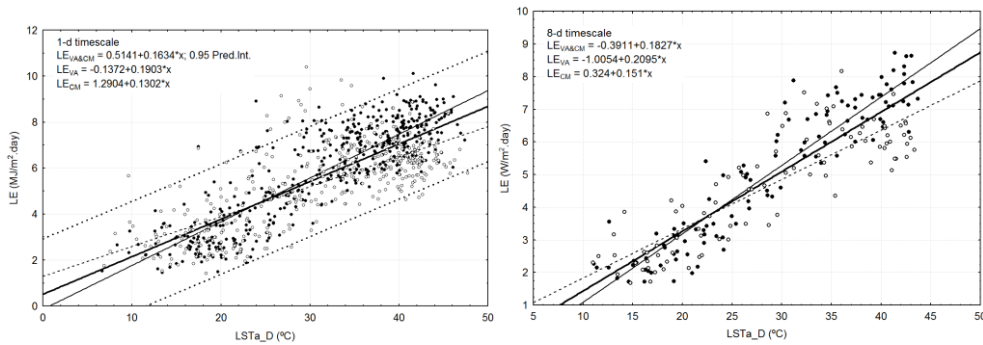


Figure 14. LST-LE relationships at Villa-Antonia and Casa-Mulero experimental stations from daily (left) and 8-day values (right).

In order to explore how the FAO crop coefficient can be predicted and be used according to Equation 1, the difference/ratio between the measured and the basal crop coefficient (here set at 0.56) was tested against ground-based and satellite-based variables.

In general, higher correlations were found when the K_c/K_{cb} was used. However, correlations were still weak being the reference evapotranspiration the best predictor among the meteorological variables ($R^2=0.34-0.38$) and land surface temperature among the satellite-based ones ($R^2=0.17-0.23$). The addition of an estimated K_c from a meteorological or satellite-based variable did not increase the predictive power of a linear regression model with LST, or E_{ref} .

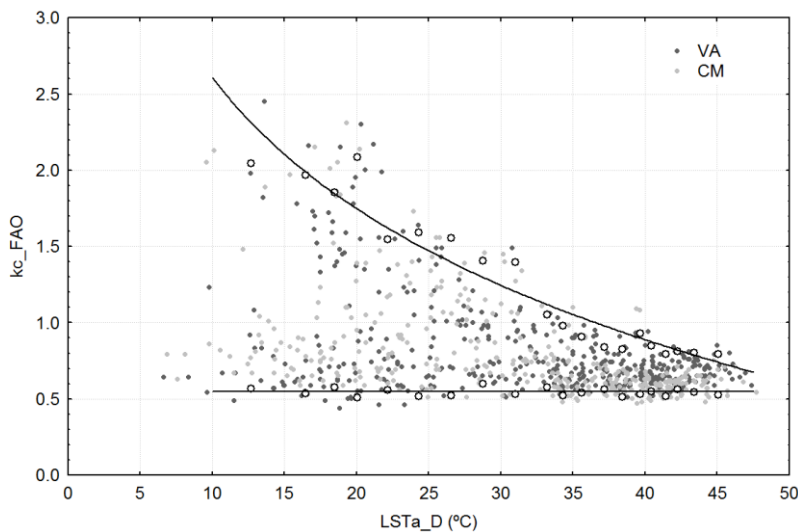


Figure 15. Threshold (P5 and P95 percentile) functions for the LSTd-crop coefficient relationship for VA and CM sites. Basal crop coefficient set at 0.62

3.4 Light Use Efficiency: temporal variability

Light Use Efficiency is defined as:



$$LUE_{gross} = \frac{GPP}{PAR * FPAR}$$

[Eq. 4]

$$LUE_{net} = \frac{NPP}{PAR * FPAR}$$

[Eq. 5]

in which,

GPP, NPP = Gross or Net Primary Production, respectively (gC/m²). Both variables were estimated from Eddy-covariance Net Ecosystem Exchange (NEE) and respiration measurements.

PAR = incoming Photosynthetically Active Radiation (MJ/m²). PAR was directly measured with a PAR-pyranometer.

FPAR = Fraction of Absorbed PAR by vegetation/canopy.

In this study FPAR has been estimated following Ogutu and Dash (Ogutu and Dash, 2013a). It states,

$$FPAR = \frac{LUE_{eco}}{iqy * fD * Eps(T)}$$

[Eq. 6]

being, LUE_{eco} the ecosystem LUE estimated as the slope of the NEE-PAR relationship, *iqy* is the intrinsic quantum yield (i.e. 0.08 mol/mol), and *fD* and *Eps(T)* are terms describing the influence of vapour pressure deficit, and leaf temperature and leaf chloroplast CO₂ partial pressure (C_i) on actual quantum yield, respectively.

$$fD = \frac{1}{1 + \exp[1.3 * (VPD_a - 3)]}$$

[Eq. 7]

$$Eps(T) = -0.0043049 * T - 0.0002077 * T^2 + 0.8973228$$

[Eq. 8]

During the inversion of NEE data, it is necessary to set an upper limit for the incident PAR to ensure that the photosynthetic capacity of vegetation is not inhibited by light saturation (Ogutu and Dash, 2013a). This threshold is set up as upper limit in PAR where the relationship with NEE ceases to be linear. In the case study this upper limit was found at 20 mol/m².day (Figure 16). Overall, estimates of FPAR were well correlated with ground-based LAI measurements at Villa Antonia field station (Figure 17).



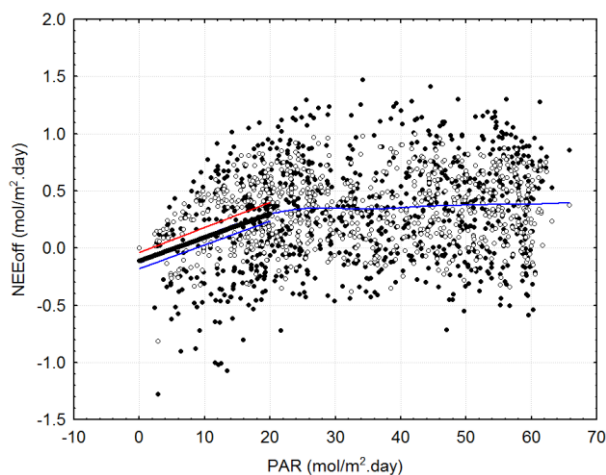


Figure 16. Relationship between daily values of PAR and NEE at Villa Antonia (filled dots) and Casa Mulero (open dots).

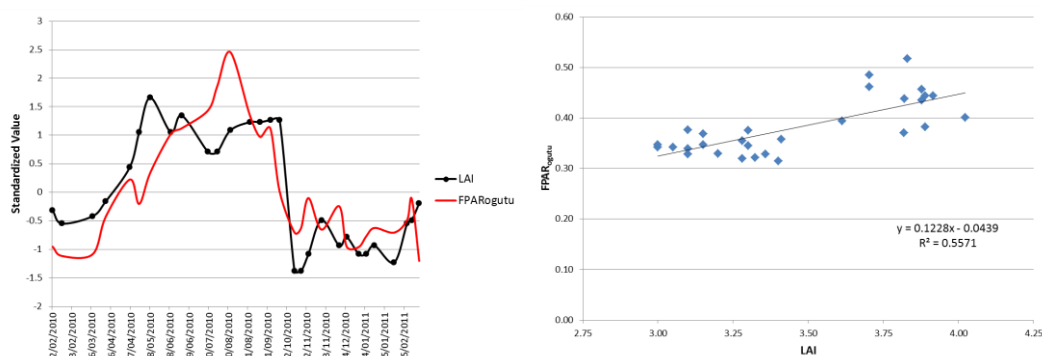


Figure 17. Comparison of ground-based LAI measurements and FPAR estimates at Villa Antonia. FPAR values computed according Ogutu & Dash (Ogutu and Dash, 2013a).

Maximum LUE_{gross} daily values were reached during the autumn and winter seasons (Figure 18, Figure 19). In VA, a 90-th percentile value of 6.6 gC/PAR was reached, while in CM was reduced by 33% (4.4 gC/MJ) (Table 9). Daily LUE_{net} maximum values were reached at winter. LUE_{net} differences in 90-th percentile-values were found to be less than with gross values, ie. 3.3 gC/MJ in VA vs 2.9 gC/MJ in CM. Overall, daily efficiencies were reduced by 10-18% when 8-day composites were considered. As representative figures of LUE values in Citrus, values of 5.5 and 3.0 gC/MJ can be set up for LUE_{gross} and LUE_{net} respectively.

Table 9. 90th-percentile values measured in Light Use Efficiencies at Citrus plots (days with negative NPP values were excluded in the analysis).

Station	LUE trait	1d-timescale	8d-timescale
VA + CM	LUE_{gross}	5.8	5.0
	LUE_{net}	3.1	2.6
VA	LUE_{gross}	6.6	5.4
	LUE_{net}	3.3	2.7
CM	LUE_{gross}	4.4	3.7
	LUE_{net}	2.9	2.6



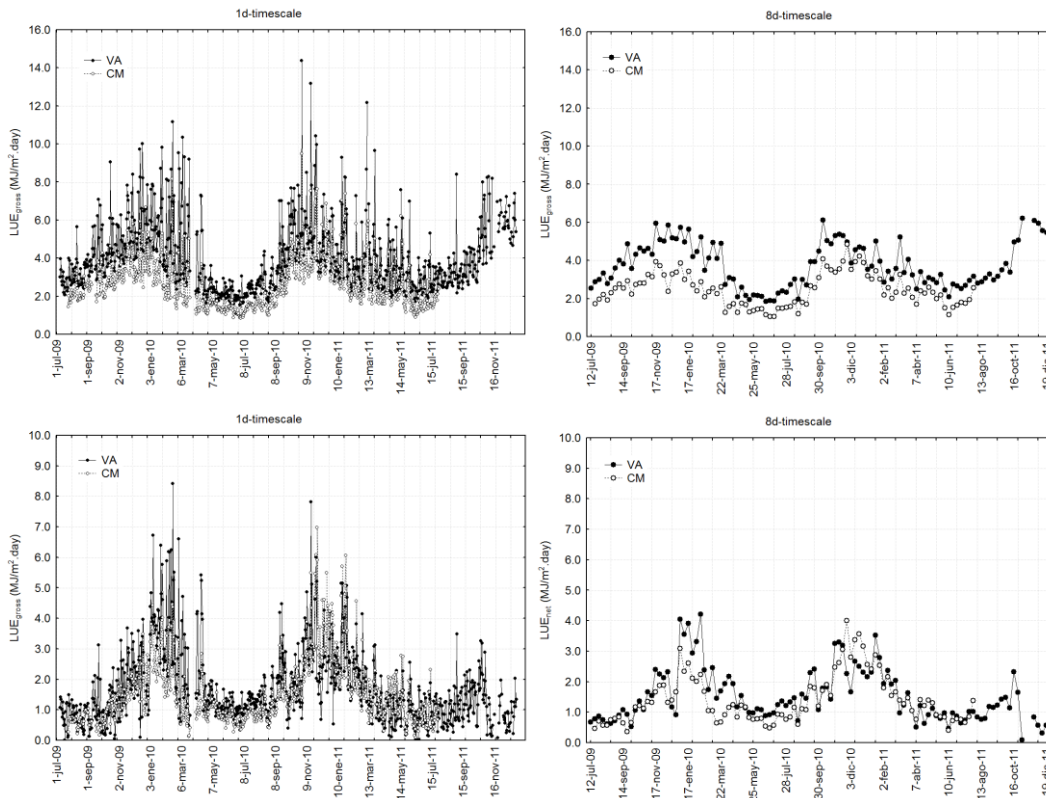


Figure 18. Seasonal variation of gross and net LUE values in Villa Antonia (VA, filled dots) and Casa Mulero (CM, open dots) experimental stations.



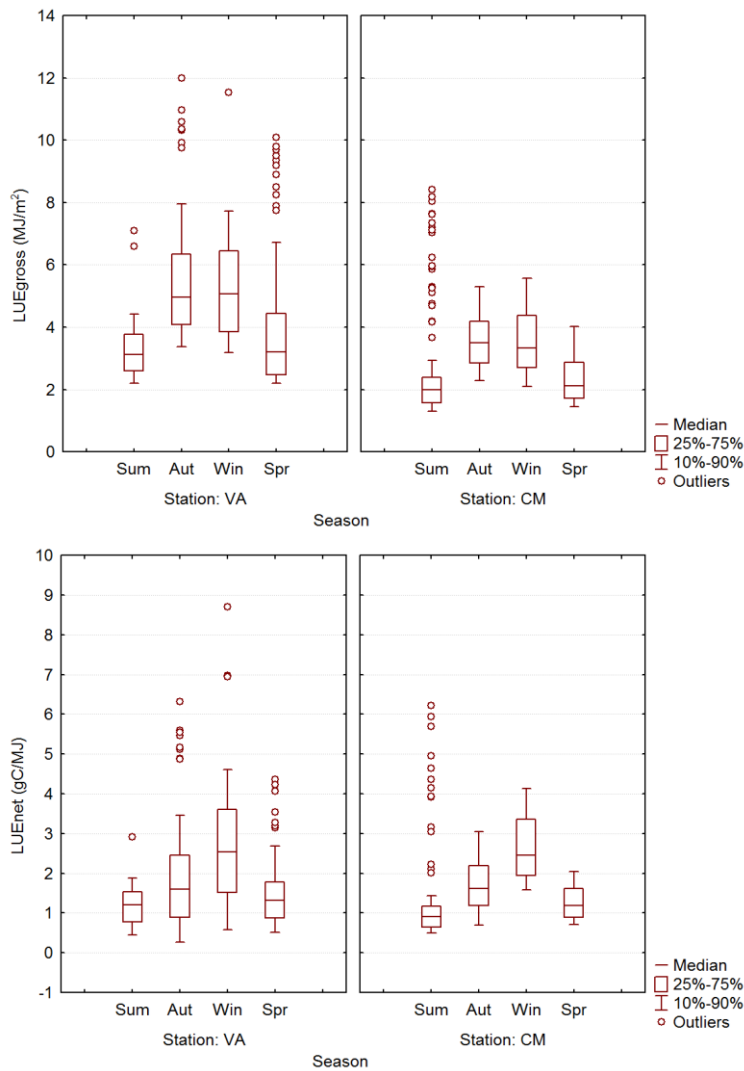


Figure 19. Boxplots with seasonal differences in Light Use Efficiency values (LUE, gC/MJ) in Villa Antonia (VA) and Casa Mulero (CM) stations. Results retrieved from the 1d-timescale dataset.

3.5 Satellite-based versus ground-based variables

The best predictor found was daytime Land Surface Temperature by Terra (LST) with moderate relationships ($R^2 = 0.58, 0.28$ and 0.50 for FPAR, LUE_{gross} and LUE_{net} , respectively) and the lowest RMSE values. Relationships were weak with NDVI with RMSE values much higher than those found with LST.



Table 10. Relationships between satellite-based variables and EC-based FPAR and LUE values.

1d-timescale		Slope	Intercept	R ²	MAE	RMSE
FPAR	NDVI	-0.4072	0.6443	0.27	0.04	0.00
	EVI	-0.0413	0.4074	0.00	0.05	0.00
	LST	51.9635	0.2504	0.58	0.03	0.00
LUE _{gross}	NDVI	14.2590	-5.5082	0.39	1.06	4.17
	EVI	8.8377	-0.7332	0.11	1.31	8.92
	LST	-0.0601	4.4955	0.28	0.76	0.87
LUE _{net}	NDVI	6.7223	-2.6065	0.22	0.72	1.02
	EVI	0.8188	1.2272	0.00	0.85	1.67
	LST	-0.0543	2.8403	0.50	0.40	0.09

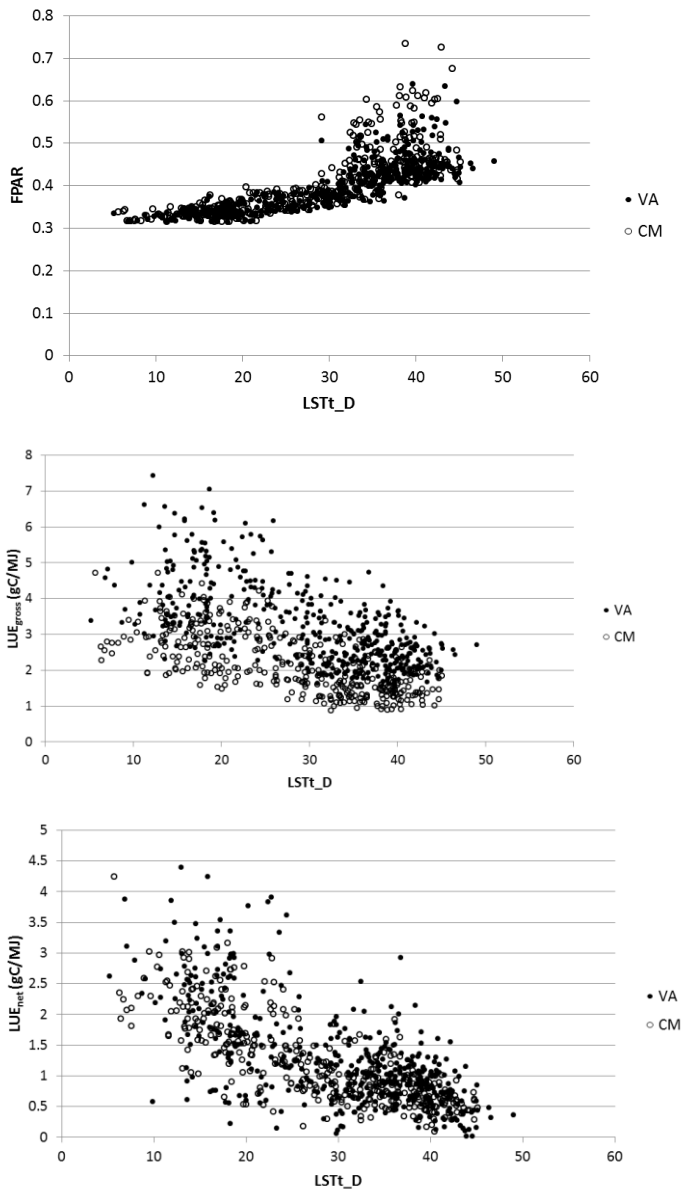


Figure 20. Scatterplots between daytime Land Surface Temperature and EC-based FPAR and LUE estimates.



3.6 Calibration of Production Efficiency Models

GPP/NPP models were calibrated and tested in their performance to explain productivity values. All tests were addressed using the 8d-timescale dataset.

3.6.1 VI model

According to Wu et al. (Wu et al., 2010c) (see section 0),

$$\text{GPP} = \text{PAR} * \text{FPAR}(\text{VI}) * \text{LUE}(\text{VI or LST})$$

[Eq. 9]

NDVI and EVI vegetation indices retrieved from MODIS were considered as potential predictors of FPAR and LUE. Additionally, the LST was evaluated as a potential predictor of LUE. NDVI, EVI and LST by alone, and the combination NDVIxNDVI, EVIxEVI, NDVIxLST, and EVIxLST were tested (Figure 21, Table 11).

LST by alone was the best predictor of GPP values in both experimental sites, explaining 85% and 76% of the variance of GPP in Villa Antonia and Casa Mulero, respectively (Table 11).

Among the different combinations of PAR*satellite-traits, the PAR*NDVI*LST contributed to explain the 76% and 67% of the GPP variance observed in Villa Antonia and Casa Mulero, respectively. However, the inclusion of satellite traits did not increase the predictability of a simple linear regression model with PAR as the only predictor. In general, the adoption of the VI*VI approach (VI model) did not provide a qualitative improvement over a SLR model in which PAR or LST act as the only predictor (see Figure 23 for the Villa Antonia case study).

Table 11. Pearson correlations (r values) between productivity values and satellite-based traits. LST refers to Day Land Surface Temperature retrieved by Terra platform. Pearson correlations consider a simple linear regression with intercept.

	VA & CM				VA				CM			
	NPPoff	GPPoff	LUEnet	LUEgross	NPPoff	GPPoff	LUEnet	LUEgross	NPPoff	GPPoff	LUEnet	LUEgross
Rgpar	0.52	0.69	-0.68	-0.74	0.55	0.84	-0.61	-0.88	0.50	0.78	-0.77	-0.85
LSTt_D	0.46	0.79	-0.69	-0.60	0.48	0.92	-0.62	-0.74	0.44	0.87	-0.77	-0.72
EVI	0.20	0.44	n.s	0.44	n.s	n.s	n.s	n.s	n.s	-0.28	0.28	n.s
NDVI	n.s.	n.s.	0.57	0.79	-0.37	-0.80	0.59	0.74	-0.23	-0.79	0.85	0.69
LSWI500	-0.35	-0.56	0.41	0.38	-0.39	-0.58	0.18	0.35	-0.32	-0.81	0.69	0.56
PAR*LST	0.49	0.73	-0.67	-0.69	0.52	0.87	-0.61	-0.84	0.48	0.82	-0.74	-0.80
PAR*EVI	0.56	0.79	-0.60	-0.57	0.56	0.81	-0.59	-0.87	0.54	0.74	-0.74	-0.85
PAR*NDVI	0.58	0.78	-0.61	-0.60	0.57	0.81	-0.60	-0.88	0.55	0.73	-0.73	-0.86
PAR*EVIxEVI	0.54	0.79	-0.48	-0.39	0.55	0.76	-0.57	-0.83	0.56	0.69	-0.69	-0.83
PAR*NDVIxNDVI	0.58	0.79	-0.46	-0.38	0.59	0.77	-0.56	-0.86	0.59	0.63	-0.63	-0.83
PAR*LSTxEVI	0.54	0.80	-0.62	-0.59	0.53	0.85	-0.60	-0.84	0.51	0.80	-0.73	-0.80
PAR*LSTxNDVI	0.54	0.81	-0.64	-0.61	0.54	0.87	-0.61	-0.84	0.52	0.81	-0.73	-0.81
EVI500*Ws_gao	-0.23	-0.41	0.24	0.18	-0.25	-0.42	n.s	n.s	-0.23	-0.66	0.47	0.30
EVI500s*Ws_gao	-0.21	-0.38	0.22	0.16	-0.22	-0.40	n.s	n.s	-0.22	-0.63	0.44	0.28
NDVI500*Ws_gao	-0.32	-0.54	0.41	0.36	-0.36	-0.58	n.s	0.30	-0.28	-0.79	0.71	0.55

EVI500 and NDVI500 represent values at the 500m spatial resolution retrieved for both experimental stations from the MOD09A1 product.

Ws_gao is the LSWI-based soil moisture scalar adopting a LSWI_{max}=1.0



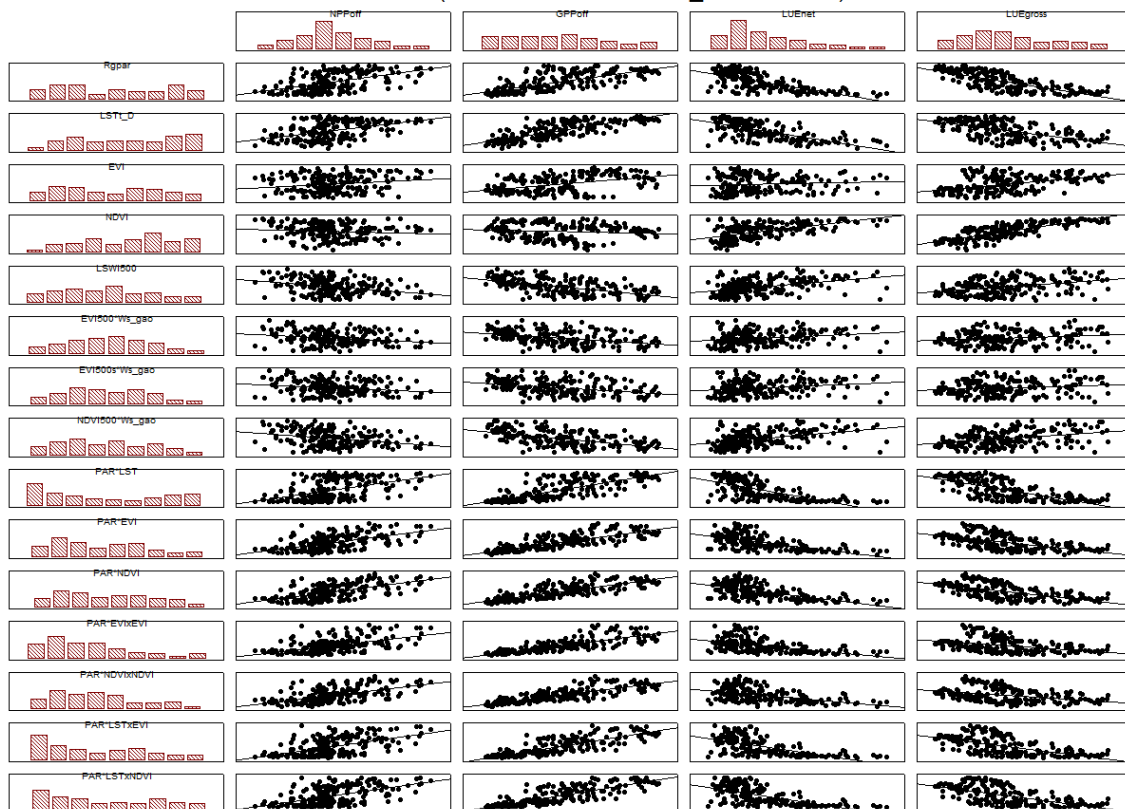


Figure 21. Matrix of scatterplots between productivity and LUE values, and satellite-based traits (alone or combined with PAR measurements). Relationships using the 8d-timescale dataset and taking the VA and CM values as a whole.

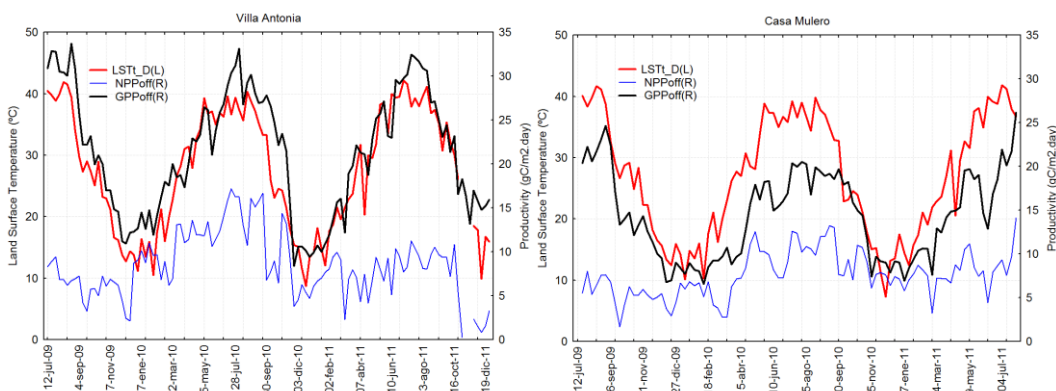


Figure 22. Seasonal dynamics of LST and productivity values at Villa Antonia (left) and Casa Mulero (right).



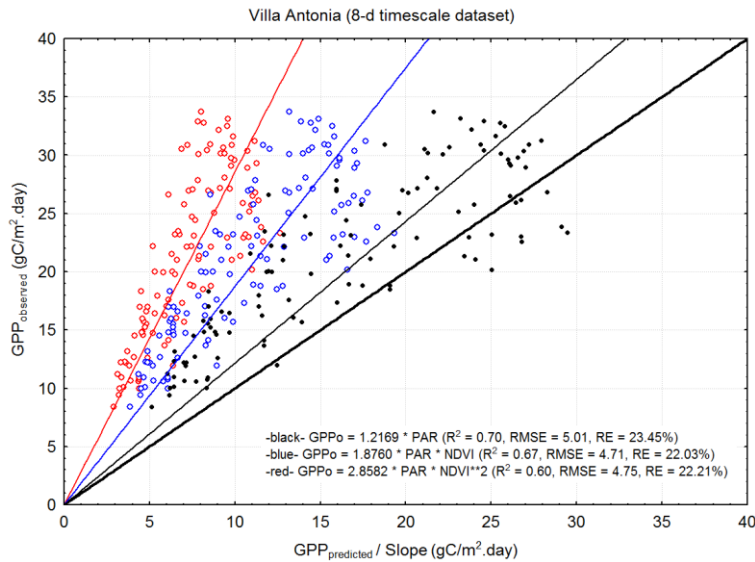


Figure 23. Calibration of no-intercept simple linear regression models for GPP estimation in Villa Antonia using PAR and NDVI as predictors. Calibration done using the 8-d timescale dataset.

3.6.2 MOD-PCM model

The MOD-PCM model uses the combined effect of a vegetation index and a LSWI-based soil moisture scalar as a surrogate of the seasonal variability of the photosynthetic capacity of the land cover, and the downward reduction of the GPP value due to the soil dryness, respectively.

The soil moisture scalar, W_{s_gao} , is computed as in the VPM model:

$$W_s = \frac{1 + LSWI}{1 + LSWI_{max}}$$

$$W_{s_gao} = \frac{1 + LSWI}{2}$$

[Eq. 10]

$$LSWI = \frac{nir - swir}{nir + swir}$$

[Eq. 11]

being, nir and $swir$ the spectral reflectances of the near infrared and short-wave infrared bands in the MODIS imagery, respectively. $LSWI_{max}$ is the maximum value reached during the growing season. Here, it is adopted a constant value of 1.0 for the $LSWI_{max}$ in a similar way than done by (Gao et al., 2014).

Timeseries of nir and $swir$ data required to compute LSWI values were retrieved from the MOD09A1 product downloaded from the University of Oklahoma Data Center (<http://www.eomf.ou.edu/modis/visualization/>). Relationships between vegetation indices and LSWI against productivity variables (GPP_{off} , NPP_{off} , LUE_{gross} , LUE_{net}) were assessed at the 500 m spatial resolution, i.e. the spatial resolution at which $swir$ reflectances are provided by MODIS.

In Figure 21 and Table 11 are shown the scatterplots and pearson correlation coefficients between productivity traits, and LSWI and combined VI- W_{s_gao} values. LSWI has a weakly-



moderately negative correlation with NPP and GPP, and positive correlation with Light Use Efficiencies.



4 Conclusions

Field and satellite-based data for the irrigated Citrus-dominated system of Villa Antonia and Casa Mulero allowed the exploration of the usefulness of simple meteorological and satellite-based variables in quantifying actual evapotranspiration rates in an operational mode. Data from both sites were analyzed on its own and together.

The trees are fully irrigated which means that both systems are mainly energy-controlled: water is not a limiting resource. This makes that the primary controls of the energy balance and actual evapotranspiration are those variables directly related with the radiative forcing of the Penman-Monteith equation. These variables include measurements of surface incoming and net radiation (highest correlation but difficult to obtain), air temperature (widely available) or temperature-based potential evapotranspiration (e.g. Hargreaves-Samani method), or satellite-based variables as Land Surface Temperature at midday. Satellite-based variables provide an interesting mean for retrieving energy turbulent fluxes in a spatially-distributed way.

The crop coefficient is difficult to predict from ancillary data. Its prediction from meteorological (e.g. air temperature, vapour pressure deficit) or satellite-based variables (land surface temperature, vegetation indices) is subject to a high uncertainty. A comparison between satellite-based vegetation indices and field-based LAI shows no relationship, suggesting that vegetation indices are not good proxies for this type of systems (fully irrigated trees).

In this study, we propose a set of empirical linear relationships for estimating daily actual evapotranspiration in irrigated Citrus-dominated agrosystems in SE Spain. These equations were calibrated at the daily and 8-day level, using the pool of total measurements taken at VA and CM sites. These local empirical equations lead to a relative error of 18% over the measured value. Besides, several Gross and Net Primary Productivity models using satellite-based variables were calibrated successfully and their performance to explain productivity values was evaluated.



5 References

- Allen, R., Irmak, A., Trezza, R., Hendrickx, J. M. H., Bastiaanssen, W. and Kjaersgaard, J.: Satellite-based ET estimation in agriculture using SEBAL and METRIC, *Hydrol. Process.*, 4027, 4011–4027, doi:10.1002/hyp, 2011.
- Allen, R. G., Pereira, L. S., Raes, D. and Smith, M.: Crop evapotranspiration, FAO technical report num. 56, Rome., 1998.
- Allen, R. G., Tasumi, M. and Trezza, R.: Satellite-Based Energy Balance for Mapping Evapotranspiration with Internalized Calibration (METRIC)—Model, *J. Irrig. Drain. Eng.*, 133(4), 380–394, doi:10.1061/(ASCE)0733-9437(2007)133:4(380), 2007.
- Asrar, G., Myneni, R. B. and Choudhury, B. J.: Spatial heterogeneity in vegetation canopies and remote sensing of absorbed photosynthetically active radiation: A modeling study, *Remote Sens. Environ.*, 41(2–3), 85–103, doi:10.1016/0034-4257(92)90070-Z, 1992.
- Bausch, W. C.: Remote sensing of crop coefficients for improving the irrigation scheduling of corn, *Agric. Water Manag.*, 27(1), 55–68, doi:10.1016/0378-3774(95)01125-3, 1995.
- Bonan, G.: *Ecological Climatology: Concepts and Applications*, 2nd ed., Cambridge University Press, Cambridge., 2008.
- Cammalleri, C. and Ciruolo, G.: A simple method to directly retrieve reference evapotranspiration from geostationary satellite images, *Int. J. Appl. Earth Obs. Geoinf.*, 21, 149–158, doi:10.1016/j.jag.2012.08.008, 2013.
- Campbell, G. S.: Extinction coefficients for radiation in plant canopies calculated using an ellipsoidal inclination angle distribution, *Agric. For. Meteorol.*, 36(4), 317–321, doi:10.1016/0168-1923(86)90010-9, 1986.
- Chen, J., Jönsson, P., Tamura, M., Gu, Z., Matsushita, B. and Eklundh, L.: A simple method for reconstructing a high-quality NDVI time-series data set based on the Savitzky–Golay filter, *Remote Sens. Environ.*, 91(3–4), 332–344, doi:10.1016/j.rse.2004.03.014, 2004.
- Chen, T., van der Werf, G. R., Dolman, A. J. and Groenendijk, M.: Evaluation of cropland maximum light use efficiency using eddy flux measurements in North America and Europe, *Geophys. Res. Lett.*, 38(14), n/a-n/a, doi:10.1029/2011GL047533, 2011.
- Churkina, G., Running, S. W., Schloss, A. L. and Intercomparison, T. P. O. T. P.: Comparing global models of terrestrial net primary productivity (NPP): The importance of water availability, *Glob. Chang. Biol.*, 5(S1), 46–55, doi:10.1046/j.1365-2486.1999.00006.x, 1999.
- Contreras, S., Hunink, J. E. and Baille, A.: Building a Watershed Information System for the Campo de Cartagena basin (Spain) integrating hydrological modeling and remote sensing, *FutureWater Report 125*, Wageningen, Netherlands., 2014.
- Coops, N. ., Waring, R. . and Landsberg, J. .: Assessing forest productivity in Australia and New Zealand using a physiologically-based model driven with averaged monthly weather data and satellite-derived estimates of canopy photosynthetic capacity, *For. Ecol. Manage.*, 104(1–3), 113–127, doi:10.1016/S0378-1127(97)00248-X, 1998.
- Courault, D., Seguin, B. and Olioso, A.: Review on estimation of evapotranspiration from remote sensing data: From empirical to numerical modeling approaches, *Irrig. Drain. Syst.*, 19(3–4), 223–249, doi:10.1007/s10795-005-5186-0, 2005.
- Cramer, W. and Field, C. B.: Comparing global models of terrestrial net primary productivity (NPP): Introduction, *Glob. Chang. Biol.*, 5(S1), iii–iv, doi:10.1046/j.1365-2486.1999.00001.x, 1999.
- Cramer, W., Kicklighter, D. W., Bondeau, A., Moore, B., Churkina, G., Nemry, B., Ruimy, A. and Schloss, A. L.: Comparing global models of terrestrial net primary productivity (NPP): Overview and key results, *Glob. Chang. Biol.*, 5(SUPPL. 1), 1–15, 1999.
- Dong, J., Xiao, X., Wagle, P., Zhang, G., Zhou, Y., Jin, C., Torn, M. S., Meyers, T. P., Suyker, A. E., Wang, J., Yan, H., Biradar, C. and Moore, B.: Comparison of four EVI-based models for estimating gross primary production of maize and soybean croplands and tallgrass prairie under severe drought, *Remote Sens. Environ.*, 162, 154–168, doi:10.1016/j.rse.2015.02.022, 2015.
- Eamus, D., Zolfaghar, S., Villalobos-Vega, R., Cleverly, J. and Huete, A.: Groundwater-dependent ecosystems: recent insights from satellite and field-based studies, *Hydrol. Earth Syst. Sci.*, in press, 2015.
- Foken, T.: The energy balance closure problem: An overview, *Ecol. Appl.*, 18(6), 1351–1367, doi:10.1890/06-0922.1, 2008.



- Gamon, J. A. and Qiu, H.: Ecological applications of remote sensing at multiple scales, edited by F. I. Pugnaire and F. Valladares, pp. 805–846, Marcel Dekker, Inc., New York., 1999.
- Gao, Y., Yu, G., Yan, H., Zhu, X., Li, S., Wang, Q., Zhang, J., Wang, Y., Li, Y., Zhao, L. and Shi, P.: A MODIS-based Photosynthetic Capacity Model to estimate gross primary production in Northern China and the Tibetan Plateau, *Remote Sens. Environ.*, 148, 108–118, doi:10.1016/j.rse.2014.03.006, 2014.
- Gebremichael, M. and Barros, A.: Evaluation of MODIS Gross Primary Productivity (GPP) in tropical monsoon regions, *Remote Sens. Environ.*, 100(2), 150–166, doi:10.1016/j.rse.2005.10.009, 2006.
- Gitelson, A. A., Viña, A., Verma, S. B., Rundquist, D. C., Arkebauer, T. J., Keydan, G., Leavitt, B., Ciganda, V., Burba, G. G. and Suyker, A. E.: Relationship between gross primary production and chlorophyll content in crops: Implications for the synoptic monitoring of vegetation productivity, *J. Geophys. Res.*, 111(D8), D08S11, doi:10.1029/2005JD006017, 2006.
- Gitelson, A. A., Peng, Y., Masek, J. G., Rundquist, D. C., Verma, S., Suyker, A., Baker, J. M., Hatfield, J. L. and Meyers, T.: Remote estimation of crop gross primary production with Landsat data, *Remote Sens. Environ.*, 121, 404–414, doi:10.1016/j.rse.2012.02.017, 2012.
- Glenn, E. P., Nagler, P. L. and Huete, A. R.: Vegetation Index Methods for Estimating Evapotranspiration by Remote Sensing, *Surv. Geophys.*, 31(6), 531–555, doi:10.1007/s10712-010-9102-2, 2010.
- Glenn, E. P., Neale, C. M. U., Hunsaker, D. J. and Nagler, P. L.: Vegetation index-based crop coefficients to estimate evapotranspiration by remote sensing in agricultural and natural ecosystems, *Hydrol. Process.*, 25(26), 4050–4062, doi:10.1002/hyp.8392, 2011.
- Goetz, S. J., Prince, S. D., Goward, S. N., Thawley, M. M. and Small, J.: Satellite remote sensing of primary production: an improved production efficiency modeling approach, *Ecol. Modell.*, 122(3), 239–255, doi:10.1016/S0304-3800(99)00140-4, 1999.
- Hargreaves, G. H. and Samani, Z. A.: Reference crop evapotranspiration from temperature, *Appl. Eng. Agric.*, 1(2), 96–99, 1985.
- Hatfield, J. ., Asrar, G. and Kanemasu, E. .: Intercepted photosynthetically active radiation estimated by spectral reflectance, *Remote Sens. Environ.*, 14(1–3), 65–75, doi:10.1016/0034-4257(84)90008-7, 1984.
- Haxeltine, A. and Prentice, I. C.: BIOME3: An equilibrium terrestrial biosphere model based on ecophysiological constraints, resource availability, and competition among plant functional types, *Global Biogeochem. Cycles*, 10(4), 693–709, doi:10.1029/96GB02344, 1996.
- Heinsch, F. A., Running, S. W., Kimball, J. S., Nemani, R. R., Davis, K. J., Bolstad, P. V., Cook, B. D., Desai, A. R., Ricciuto, D. M., Law, B. E., Oechel, W. C., Wofsy, S. C., Dunn, A. L., Munger, J. W., Baldocchi, D. D., Hollinger, D. Y., Richardson, A. D., Stoy, P. C., Siqueira, M. B. S., Monson, R. K., Burns, S. P. and Flanagan, L. B.: Evaluation of remote sensing based terrestrial productivity from MODIS using regional tower eddy flux network observations, *IEEE Trans. Geosci. Remote Sens.*, 44(7), 1908–1925, doi:10.1109/TGRS.2005.853936, 2006.
- Hunink, J. E., Contreras, S., Soto-García, M., Martin-Gorrioz, B., Martínez-Álvarez, V. and Baille, A.: Estimating groundwater use patterns of perennial and seasonal crops in a Mediterranean irrigation scheme, using remote sensing, *Agric. Water Manag.*, 162, 47–56, doi:10.1016/j.agwat.2015.08.003, 2015.
- Hunink, J. E., Eekhout, J. P. C., Vente, J. De, Contreras, S., Droogers, P. and Baille, A.: Hydrological Modelling using Satellite-Based Crop Coefficients : A Comparison of Methods at the Basin Scale, , 1–16, doi:10.3390/rs9020174, 2017.
- Huntzinger, D. N., Post, W. M., Wei, Y., Michalak, A. M., West, T. O., Jacobson, A. R., Baker, I. T., Chen, J. M., Davis, K. J., Hayes, D. J., Hoffman, F. M., Jain, A. K., Liu, S., McGuire, A. D., Neilson, R. P., Potter, C., Poulter, B., Price, D., Raczka, B. M., Tian, H. Q., Thornton, P., Tomelleri, E., Viovy, N., Xiao, J., Yuan, W., Zeng, N., Zhao, M. and Cook, R.: North American Carbon Program (NACP) regional interim synthesis: Terrestrial biospheric model intercomparison, *Ecol. Modell.*, 232, 144–157, doi:10.1016/j.ecolmodel.2012.02.004, 2012.
- Jin, C., Xiao, X., Wagle, P., Griffis, T., Dong, J., Wu, C., Qin, Y. and Cook, D. R.: Effects of in-situ and reanalysis climate data on estimation of cropland gross primary production using the Vegetation Photosynthesis Model, *Agric. For. Meteorol.*, 213, 240–250,



- doi:10.1016/j.agrformet.2015.07.003, 2015.
- Jönsson, P. and Eklundh, L.: Seasonality Extraction by Function Fitting to Time-Series of Satellite Sensor Data, *IEEE Trans. Geosci. Remote Sens.*, 40(8), 1824–1832, doi:10.1109/TGRS.2002.802519, 2002.
- Jönsson, P. and Eklundh, L.: TIMESAT—a program for analyzing time-series of satellite sensor data, *Comput. Geosci.*, 30(8), 833–845, doi:10.1016/j.cageo.2004.05.006, 2004.
- Kalfas, J. L., Xiao, X., Vanegas, D. X., Verma, S. B. and Suyker, A. E.: Modeling gross primary production of irrigated and rain-fed maize using MODIS imagery and CO₂ flux tower data, *Agric. For. Meteorol.*, 151(12), 1514–1528, doi:10.1016/j.agrformet.2011.06.007, 2011.
- Kalma, J. D., McVicar, T. R. and McCabe, M. F.: Estimating land surface evaporation: A review of methods using remotely sensed surface temperature data, *Surv. Geophys.*, 29, 421–469, 2008.
- Kamble, B., Irmak, A. and Hubbard, K.: Estimating Crop Coefficients Using Remote Sensing-Based Vegetation Index, *Remote Sens.*, 5(4), 1588–1602, doi:10.3390/rs5041588, 2013.
- Kanniah, K. D., Beringer, J., Hutley, L. B., Tapper, N. J. and Zhu, X.: Evaluation of Collections 4 and 5 of the MODIS Gross Primary Productivity product and algorithm improvement at a tropical savanna site in northern Australia, *Remote Sens. Environ.*, 113(9), 1808–1822, doi:10.1016/j.rse.2009.04.013, 2009.
- Kelley, D. I., Prentice, I. C., Harrison, S. P., Wang, H., Simard, M., Fisher, J. B. and Willis, K. O.: A comprehensive benchmarking system for evaluating global vegetation models, *Biogeosciences*, 10(5), 3313–3340, doi:10.5194/bg-10-3313-2013, 2013.
- Knorr, W. and Heimann, M.: Impact of drought stress and other factors on seasonal land biosphere CO₂ exchange studied through an atmospheric tracer transport model, *Tellus, Ser. B*, 47 B(4), 471–489, 1995.
- Landsberg, J. J. and Waring, R. H.: A generalised model of forest productivity using simplified concepts of radiation-use efficiency, carbon balance and partitioning, *For. Ecol. Manage.*, 95(3), 209–228, doi:10.1016/S0378-1127(97)00026-1, 1997.
- Li, Z.-L., Tang, R., Wan, Z., Bi, Y., Zhou, C., Tang, B., Yan, G. and Zhang, X.: A Review of Current Methodologies for Regional Evapotranspiration Estimation from Remotely Sensed Data, *Sensors*, 9(5), 3801–3853, doi:10.3390/s90503801, 2009.
- Liu, Z., Wang, L. and Wang, S.: Comparison of different GPP models in China using MODIS image and ChinaFLUX data, *Remote Sens.*, 6(10), 10215–10231, doi:10.3390/rs61010215, 2014.
- Maeda, E. E., Wiberg, D. A. and Pellikka, P. K. E.: Estimating reference evapotranspiration using remote sensing and empirical models in a region with limited ground data availability in Kenya, *Appl. Geogr.*, 31(1), 251–258, doi:10.1016/j.apgeog.2010.05.011, 2011.
- Makkink, G.: Testing the Penman formula by means of lysimeters, *J. Inst. Water Eng.*, 11, 277–288, 1957.
- Martin-Gorriz, B., Egea, G., Nortes, P. A., Baille, A., González-Real, M. M., Ruiz-Salleres, I. and Verhoef, A.: Effects of high temperature and vapour pressure deficit on net ecosystem exchange and energy balance of an irrigated orange orchard in a semi-Arid climate (Southern Spain), in *Acta Horticulturae*, vol. 922, pp. 149–156., 2011.
- Mateos, L., González-Dugo, M. P., Testi, L. and Villalobos, F. J.: Monitoring evapotranspiration of irrigated crops using crop coefficients derived from time series of satellite images. I. Method validation, *Agric. Water Manag.*, 125, 81–91, doi:10.1016/j.agwat.2012.11.005, 2013.
- McCallum, I., Wagner, W., Schmullius, C., Shvidenko, A., Obersteiner, M., Fritz, S. and Nilsson, S.: Satellite-based terrestrial production efficiency modeling, *Carbon Balance Manag.*, 4, 8, doi:10.1186/1750-0680-4-8, 2009.
- Monteith, J. L. and Moss, C. J.: Climate and the Efficiency of Crop Production in Britain, *Philos. Trans. R. Soc. B Biol. Sci.*, 281(980), 277–294, doi:10.1098/rstb.1977.0140, 1977.
- Nagler, P., Scott, R., Westenburg, C., Cleverly, J., Glenn, E. and Huete, A.: Evapotranspiration on western U.S. rivers estimated using the Enhanced Vegetation Index from MODIS and data from eddy covariance and Bowen ratio flux towers, *Remote Sens. Environ.*, 97(3), 337–351, doi:10.1016/j.rse.2005.05.011, 2005.
- Nagler, P., Glenn, E., Nguyen, U., Scott, R. and Doody, T.: Estimating Riparian and Agricultural Actual Evapotranspiration by Reference Evapotranspiration and MODIS Enhanced Vegetation Index, *Remote Sens.*, 5(8), 3849–3871, doi:10.3390/rs5083849, 2013.
- Nguy-Robertson, A., Suyker, A. and Xiao, X.: Modeling gross primary production of maize and



- soybean croplands using light quality, temperature, water stress, and phenology, *Agric. For. Meteorol.*, 213, 160–172, doi:10.1016/j.agrformet.2015.04.008, 2015.
- Ogutu, B. O. and Dash, J.: An algorithm to derive the fraction of photosynthetically active radiation absorbed by photosynthetic elements of the canopy (FAPAR(ps)) from eddy covariance flux tower data., *New Phytol.*, 197(2), 511–23, doi:10.1111/nph.12039, 2013a.
- Ogutu, B. O. and Dash, J.: Assessing the capacity of three production efficiency models in simulating gross carbon uptake across multiple biomes in conterminous USA, *Agric. For. Meteorol.*, 174–175, 158–169, doi:10.1016/j.agrformet.2013.02.016, 2013b.
- Parton, W. J.: Observations and modeling of biomass and soil organic matter dynamics for the grassland biome worldwide, *Global Biogeochem. Cycles*, 7(4), 785–809, 1993.
- Peng, Y., Gitelson, A. A., Keydan, G., Rundquist, D. C. and Moses, W.: Remote estimation of gross primary production in maize and support for a new paradigm based on total crop chlorophyll content, *Remote Sens. Environ.*, 115(4), 978–989, doi:10.1016/j.rse.2010.12.001, 2011.
- Pereira, L. S., Allen, R. G., Smith, M. and Raes, D.: Crop evapotranspiration estimation with FAO56: Past and future, *Agric. Water Manag.*, 147, 4–20, doi:10.1016/j.agwat.2014.07.031, 2014.
- Petillo, M. G. and Castel, J. R.: Water balance and crop coefficient estimation of a citrus orchard in Uruguay, , 5(2), 232–243, 2007.
- Potter, C. S.: Terrestrial ecosystem production: a process model based on global satellite and surface data, *Global Biogeochem. Cycles*, 7(4), 811–841, 1993.
- Priestley, C. H. B. and Taylor, R. J.: On the assessment of surface heat flux and evaporation using large scale parameters, *Mon. Weather Rev.*, 100(2), 81–92, 1972.
- Prince, S. D.: A model of regional primary production for use with coarse resolution satellite data, *Int. J. Remote Sens.*, 12(6), 1313–1330, doi:10.1080/01431169108929728, 1991.
- Prince, S. D. and Goward, S. N.: Global primary production: a remote sensing approach, *J. Biogeogr.*, 22(4–5), 815–835, 1995.
- Raich, J. W.: Potential net primary productivity in South America: application of a global model, *Ecol. Appl.*, 1(4), 399–429, 1991.
- Ruimy, A., Dedieu, G. and Saugier, B.: TURC: A diagnostic model of continental gross primary productivity and net primary productivity, *Global Biogeochem. Cycles*, 10(2), 269–285, doi:10.1029/96GB00349, 1996.
- Ruimy, A., Kergoat, L., Bondeau, A. and Intercomparison, T. P. O. T. P.: Comparing global models of terrestrial net primary productivity (NPP): analysis of differences in light absorption and light-use efficiency, *Glob. Chang. Biol.*, 5(S1), 56–64, doi:10.1046/j.1365-2486.1999.00007.x, 1999.
- Running, S. W. and Zhao, M.: Daily GPP and Annual NPP (MOD17A2/A3) products NASA Earth Observing System MODIS Land Algorithm - User's guide V3., 2015.
- Sasai, T., Ichii, K., Yamaguchi, Y. and Nemani, R.: Simulating terrestrial carbon fluxes using the new biosphere model "biosphere model integrating eco-physiological and mechanistic approaches using satellite data" (BEAMS), *J. Geophys. Res.*, 110(G2), G02014, doi:10.1029/2005JG000045, 2005.
- Sims, D., Rahman, A., Cordova, V., Elmasri, B., Baldocchi, D., Bolstad, P., Flanagan, L., Goldstein, A., Hollinger, D. and Misson, L.: A new model of gross primary productivity for North American ecosystems based solely on the enhanced vegetation index and land surface temperature from MODIS, *Remote Sens. Environ.*, 112(4), 1633–1646, doi:10.1016/j.rse.2007.08.004, 2008.
- Singh, R. and Irmak, A.: Estimation of Crop Coefficients Using Satellite Remote Sensing, *J. Irrig. Drain. Eng.*, 135(5), 597–608, doi:10.1061/(ASCE)IR.1943-4774.0000052, 2009.
- Sjöström, M., Zhao, M., Archibald, S., Arneeth, A., Cappelaere, B., Falk, U., de Grandcourt, A., Hanan, N., Kergoat, L., Kutsch, W., Merbold, L., Mougou, E., Nickless, A., Nouvellon, Y., Scholes, R. J., Veenendaal, E. M. and Ardö, J.: Evaluation of MODIS gross primary productivity for Africa using eddy covariance data, *Remote Sens. Environ.*, 131, 275–286, doi:10.1016/j.rse.2012.12.023, 2013.
- Smets, B., Swinnen, E. and Van Hoolst, R.: GIOGL1 Dry Matter Productivity. Product User Manual, Version 1 (12.10)., 2016.
- Szilagy, J.: Testing the Rationale behind an Assumed Linear Relationship between Evapotranspiration and Land Surface Temperature, *J. Hydrol. Eng.*, 20(5), 4014073, doi:10.1061/(ASCE)HE.1943-5584.0001091, 2015.
- Tan, K. P., Kanniah, K. D. and Cracknell, A. P.: A review of remote sensing based productivity



- models and their suitability for studying oil palm productivity in tropical regions, *Prog. Phys. Geogr.*, 36(5), 655–679, doi:10.1177/0309133312452187, 2012.
- Tang, X., Li, H., Huang, N., Li, X., Xu, X., Ding, Z. and Xie, J.: A comprehensive assessment of MODIS-derived GPP for forest ecosystems using the site-level FLUXNET database, *Environ. Earth Sci.*, 74(7), 5907–5918, doi:10.1007/s12665-015-4615-0, 2015.
- Turner, D. P., Ritts, W. D., Cohen, W. B., Gower, S. T., Running, S. W., Zhao, M., Costa, M. H., Kirschbaum, A. A., Ham, J. M., Saleska, S. R. and Ahl, D. E.: Evaluation of MODIS NPP and GPP products across multiple biomes, *Remote Sens. Environ.*, 102(3–4), 282–292, doi:10.1016/j.rse.2006.02.017, 2006.
- Twine, T. E., Kustas, W. P., Norman, J. M., Cook, D. R., Houser, P. R., Meyers, T. P., Prueger, J. H., Starks, P. J. and Wesely, M. L.: Correcting eddy-covariance flux underestimates over a grassland, *Agric. For. Meteorol.*, 103(3), 279–300, doi:10.1016/S0168-1923(00)00123-4, 2000.
- Venturini, V., Islam, S. and Rodriguez, L.: Estimation of evaporative fraction and evapotranspiration from MODIS products using a complementary based model, *Remote Sens. Environ.*, 112(1), 132–141, doi:10.1016/j.rse.2007.04.014, 2008.
- Veroustraete, F., Sabbe, H. and Eerens, H.: Estimation of carbon mass fluxes over Europe using the C-Fix model and Euroflux data, *Remote Sens. Environ.*, 83(3), 376–399, doi:10.1016/S0034-4257(02)00043-3, 2002.
- Wagle, P., Xiao, X. and Suyker, A. E.: Estimation and analysis of gross primary production of soybean under various management practices and drought conditions, *ISPRS J. Photogramm. Remote Sens.*, 99, 70–83, doi:10.1016/j.isprsjprs.2014.10.009, 2015.
- Wang, K., Li, Z. and Cribb, M.: Estimation of evaporative fraction from a combination of day and night land surface temperatures and NDVI: A new method to determine the Priestley–Taylor parameter, *Remote Sens. Environ.*, 102(3–4), 293–305, doi:10.1016/j.rse.2006.02.007, 2006.
- Wang, W., Duncan, J., Hashimoto, H., Michaelis, A. R., Milesi, C., Ichiim, K. and Nemani, R. R.: Diagnosing and assessing uncertainties of terrestrial ecosystem models in a multimodel ensemble experiment: 1. Primary production, *Glob. Chang. Biol.*, 17(3), 1350–1366, doi:10.1111/j.1365-2486.2010.02309.x, 2011.
- Wiegand, C. L., Richardson, A. J., Escobar, D. E. and Gerbermann, A. H.: Vegetation indices in crop assessments, *Remote Sens. Environ.*, 35(2–3), 105–119, doi:10.1016/0034-4257(91)90004-P, 1991.
- Wilson, K., Goldstein, A., Falge, E., Aubinet, M., Baldocchi, D., Berbigier, P., Bernhofer, C., Ceulemans, R., Dolman, H., Field, C., Grelle, A., Ibrom, A., Law, B., Kowalski, A., Meyers, T., Moncrieff, J., Monson, R., Oechel, W., Tenhunen, J., Valentini, R. and Verma, S.: Energy balance closure at FLUXNET sites, *Agric. For. Meteorol.*, 113(1–4), 223–243, doi:10.1016/S0168-1923(02)00109-0, 2002.
- Wu, C., Munger, J. W., Niu, Z. and Kuang, D.: Comparison of multiple models for estimating gross primary production using MODIS and eddy covariance data in Harvard Forest, *Remote Sens. Environ.*, 114(12), 2925–2939, doi:10.1016/j.rse.2010.07.012, 2010a.
- Wu, C., Han, X., Ni, J., Niu, Z. and Huang, W.: Estimation of gross primary production in wheat from in situ measurements, *Int. J. Appl. Earth Obs. Geoinf.*, 12(3), 183–189, doi:10.1016/j.jag.2010.02.006, 2010b.
- Wu, C., Niu, Z. and Gao, S.: Gross primary production estimation from MODIS data with vegetation index and photosynthetically active radiation in maize, *J. Geophys. Res.*, 115(D12), D12127, doi:10.1029/2009JD013023, 2010c.
- Wu, C., Chen, J. M. and Huang, N.: Predicting gross primary production from the enhanced vegetation index and photosynthetically active radiation: Evaluation and calibration, *Remote Sens. Environ.*, 115(12), 3424–3435, doi:10.1016/j.rse.2011.08.006, 2011.
- Xiao, X., Hollinger, D., Aber, J., Goltz, M., Davidson, E. A., Zhang, Q. and Moore, B.: Satellite-based modeling of gross primary production in an evergreen needleleaf forest, *Remote Sens. Environ.*, 89(4), 519–534, doi:10.1016/j.rse.2003.11.008, 2004.
- Xiao, X., Zhang, Q., Saleska, S., Hutyrá, L., De Camargo, P., Wofsy, S., Froking, S., Boles, S., Keller, M. and Moore, B.: Satellite-based modeling of gross primary production in a seasonally moist tropical evergreen forest, *Remote Sens. Environ.*, 94(1), 105–122, doi:10.1016/j.rse.2004.08.015, 2005.
- Xin, Q., Broich, M., Suyker, A. E., Yu, L. and Gong, P.: Multi-scale evaluation of light use efficiency in MODIS gross primary productivity for croplands in the Midwestern United States, *Agric. For. Meteorol.*, 201, 111–119, doi:10.1016/j.agrformet.2014.11.004, 2015.



- Xing, Z., Chow, L., Meng, F. R., Rees, H. W., Stevens, L. and Monteith, J.: Validating evapotranspiration equations using bowen ratio in New Brunswick, Maritime, Canada, *Sensors*, 8(1), 412–428, 2008.
- Yang, Y., Shang, S., Guan, H. and Jiang, L.: A novel algorithm to assess gross primary production for terrestrial ecosystems from MODIS imagery, *J. Geophys. Res. Biogeosciences*, 118(2), 590–605, doi:10.1002/jgrg.20056, 2013.
- Yuan, W., Liu, S., Zhou, G., Zhou, G., Tieszen, L. L., Baldocchi, D., Bernhofer, C., Gholz, H., Goldstein, A. H., Goulden, M. L., Hollinger, D. Y., Hu, Y., Law, B. E., Stoy, P. C., Vesala, T. and Wofsy, S. C.: Deriving a light use efficiency model from eddy covariance flux data for predicting daily gross primary production across biomes, *Agric. For. Meteorol.*, 143(3–4), 189–207, doi:10.1016/j.agrformet.2006.12.001, 2007.
- Zhao, M., Heinsch, F. A., Nemani, R. R. and Running, S. W.: Improvements of the MODIS terrestrial gross and net primary production global data set, *Remote Sens. Environ.*, 95(2), 164–176, doi:10.1016/j.rse.2004.12.011, 2005.



Appendix I: Satellite-based Production Efficiency Models

An overview is provided of the principal satellite data-based Production Efficiency Models.

CASA (Carnegie Ames Stanford Approach)

Source: (Potter, 1993).

CASA estimates NPP directly using a numerical model of monthly fluxes of water, carbon and nitrogen in terrestrial ecosystems. Estimates of terrestrial NPP fluxes depend on inputs of global satellite observations for land surface properties and on gridded model drivers from interpolated weather station records. The calibrated model has been assessed globally. A constant LUE_{max} value of 0.389 gC/MJ is adopted, and stress scalars depend on temperature and soil moisture conditions.

In CASA, the temperature stress scalar is derived considering optimal temperatures for plant production, while the water stress scalar is estimated as the monthly water deficit computed from a comparison of the moisture supply and the potential evapotranspiration demand figures.

SDBM (Simple Diagnostic Biosphere Model)

Source: (Knorr and Heimann, 1995).

NPP is estimated monthly from climate data, observed greenness from vegetation index data, and a drought-stress scalar which equals the Priestley-Taylor ratio in an hypothetical one-layer bucket model. A LUE_{max} constant value of 1.00 gC/MJ is adopted.

$$NPP = PAR * FPAR * LUE_{max} * D_s$$

in which,

FPAR is computed using a linear relationship function with the NDVI vegetation index.

$$FPAR = 2.186 * NDVI - 0.1913$$

[Eq. 12]

$$D_s = \frac{ET_a}{ET_{eq}}$$

[Eq. 13]

being

D_s the Priestley-Taylor ratio computed as the ratio of actual to equilibrium evapotranspiration.

SDBM computes the Net Ecosystem Productivity as the difference between NPP and the soil-heterotrophic respiration, as

$$NEP = NPP - R_h$$

in which, R_h is modeled as a function of temperature and water availability. R_h is assumed to be equal to NPP at the end of each year (this implies that the respiring pool of soil carbon is in equilibrium at the annual scale).

$$R_h = \beta * Q_{10}^{T/10} * D_s$$

$$Q_{10} = 1.5$$

T is the air surface temperature, and β is calibrated for reaching $NPP=R_h$ at the end of the year



TURC

Source: (Ruimy et al., 1996).

This model includes a soil water deficit scalar (SWD) as a primary stressor in controlling productivity in drier regions. A LUE_{max} constant value of 1.10 gC/MJ is adopted.

$$FPAR = 1.25 * NDVI - 0.025$$

Respiration: Autotrophic-maintenance respiration (R_{aM}) and growth respiration (R_{aG}).

$MR = f(T, vegC)$; $vegC$ = maintenance coeff. depending on C pool-type (leaves, fine roots, sapwood)

$$GR = 0.28 * (GPP - R_{aM})$$

NPP is finally computed as

$$NPP = 0.72 * (GPP - R_{aM})$$

C-Fix

Source: (Veroustraete et al., 2002).

C-Fix estimates daily ecosystem productivity ranging from local to global scale by using three inputs, namely solar radiation, temperature and APAR. A LUE_{max} constant value of 1.10 gC/MJ is adopted. After, NPP is computed as the difference between GPP and R_a (autotrophic respiration), and NEP as NPP less R_h (heterotrophic respiration). At the present, C-Fix has been adopted by the Copernicus system to provide global NPP estimates (maps of NPP, called Dry Matter Productivity, is available since 1998 and can be accessed from [here](#)). In the operational system, several simplifications have been adopted over the original formulation (Smets et al., 2016).

LUE scalars: Temperature (normalized temperature dependency factor, $p(T_c)$), Soil moisture (it controls the Radiation Use Efficiency/LUE, RUE), CO_2 - fertilization.

Respiration: It is a fraction of GPP which depends on: 1) an allometric factor (carbon release ratio between leaves to roots), and 2) a respiratory fraction based on air temperature

3-PGS (3-Physiological Principles Predicting Growth using Satellites)

Source: (Coops et al., 1998).

The 3-PGS model is a modified version of the dynamical vegetation 3-PG model originally developed by Landsberg and Waring (1997). 3-PGS runs monthly, and uses a constant LUE_{max} (1.8 gC/MJ²) and inputs of meteorological data (e.g. temperature, VPD, rainfall and frost), soil information (e.g. fertility and soil moisture) and biophysical parameters (e.g. fPAR and physiological information) to estimate vegetation productivity.

$$GPP = PAR(T_{min}, T_{max}) * FPAR(NDVI) * LUE_{max} * Scalars$$

Scalars: Frost days, Soil Water Deficit, VPD

$$NPP = 0.45 * GPP$$



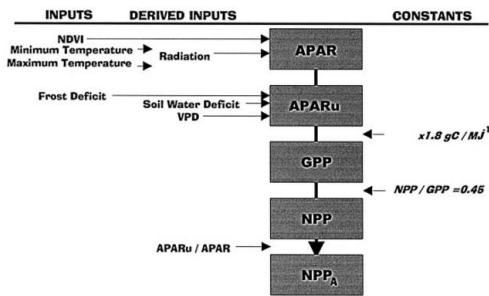


Figure 24. Diagrammatic representation of the 3-PGS model (taken from Coops et al. (Coops et al., 1998)).

GLO-PEM

Source: (Prince and Goward, 1995).

It was designed to run with both biological and environmental variables derived entirely from satellites. However, it requires to quantify the relative contribution of C3 and C4 vegetation by pixel. This is computed as a function of above ground biomass estimated from the minimum annual visible channel reflectance and the air temperature.

GLO-PEM estimates LUE_{max} values rather than using prescribing values.

LUE scalars: Air temperature, VPD, and Soil moisture.

Respiration: Autotrophic respiration is modeled for maintenance respiration (R_{am}) using a semi-empirical relationship as a function of vegetation, biomass, air temperature and photosynthetic rate; Growth respiration (R_{ag}) is a constant of GPP (0.25). Below-ground biomass is not estimated, thus R_a is assumed to apply to the whole plant.

MOD17

MODIS primary production products (MOD17) are the first regular, near-real-time data sets for repeated monitoring of vegetation primary production on vegetated land at 1-km resolution at an 8-day interval (Zhao et al., 2005). MOD17 does not rely on empirically defined vegetation indices, but attempts to model the biochemical and physical processes involved in photosynthesis. The MOD17 is operational at a global scale utilizing a modified version of the LUE algorithms and three upstream inputs, MODIS land-cover products (MOD12), LAI/fPAR (MOD15), and daily meteorological data from the Global Modeling and Assimilation Office (GMAO) (Running and Zhao, 2015). GPP is estimated at daily scale, while NPP is computed annually (Figure 25).



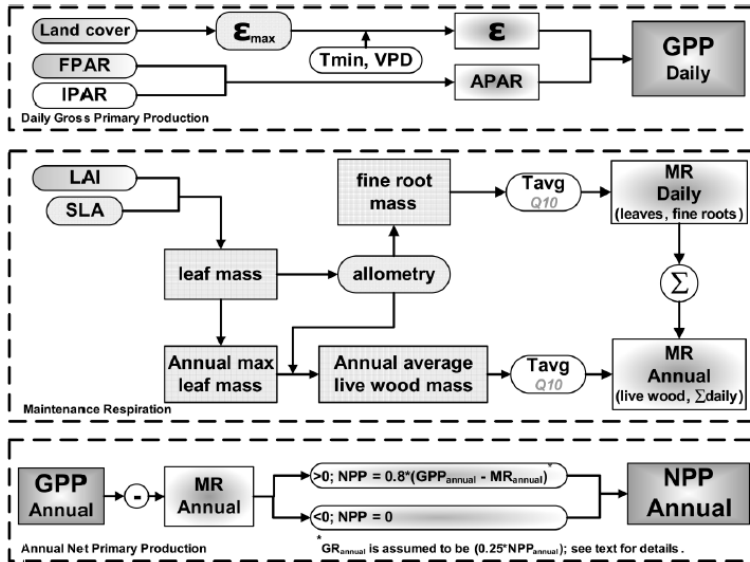


Figure 25. Conceptual structure of MOD17 algorithm (taken from Running and Zhao (Running and Zhao, 2015))

Daily GPP estimation:

It uses [Eq. 1], being

$$PAR = 0.45 * R_s$$

FPAR is taken from MOD15, in which $FPAR = a * VI + b$.

LUE scalars: Minimum temperature (T_{min}), Vapour Pressure Deficit (VPD).

Source of weather inputs: PAR, T_{min} , VDP provided by GMAO (Global Modeling and Assimilation Office)

LUE_{max} , VPD and T threshold values are derived from outputs of the BIOME-BGC model and summarized in the MOD12 Biome Properties Look-Up Table.

Only 8-day accumulated values are provided to the public. The summations are named for the first day included in the 8-day period.

Daily MR and PSN_{net} estimation:

Daily Net Photosynthesis (PSN_{net}) is estimated as the difference between daily GPP and daily maintenance respiration (MR). PSN_{net} does not include *maintenance respiration associated with live wood (Livewood_MR)*, nor does it include *growth respiration (GR)*.

Daily MR is diverted into respiration driven by roots (Froot_MR) and leaves (Leaf_MR). Both are computed based on an exponential function of average daily temperature and scaled down by leaf mass, i.e. the LAI/SLA ratio (SLA = Specific Leaf Area). LAI is extracted from MOD15 and SLA from MOD12-BPLUTs

$$PSN_{net} = GPP - Leaf_MR - Froot_MR$$

$$Leaf_MR = Leaf_Mass * leaf_mr_base * Q10_mr^{**}[(T_{avg}-20)/10]$$

$$Froot_MR = Leaf_Mass * froot_leaf_ratio * froot_mr_base * Q10_mr^{**}[(T_{avg}-20)/10]$$



$$\text{Leaf_Mass} = \text{LAI} / \text{SLA}$$

Finally, PSN_{net} can be extracted as

$$\text{PSN}_{\text{net}} = \text{GPP} - \text{Leaf_Mass} * \text{Q10_mr}^{**}[(T_{\text{avg}}-20)/10] * (\text{leaf_mr_base} + \text{froot_leaf_ratio} * \text{froot_mr_base})$$

As for GPP, only 8-day accumulated values of PSN_{net} values are provided to the public. The summations are named for the first day included in the 8-day period.

Annual NPP estimation:

$$\text{NPP}_{\text{annual}} = \Sigma \text{GPP}_{\text{day}} - [\Sigma \text{Leaf_MR} + \Sigma \text{Froot_MR} + \text{Lwood_MR}_{\text{annual}}] - \text{GR}_{\text{annual}}$$

$$\text{NPP}_{\text{annual}} = \text{GPP}_{\text{annual}} - \text{MR}_{\text{annual}} - \text{GR}_{\text{annual}}$$

From Running and Zhao (Running and Zhao, 2015),

$$\text{If } (\text{GPP}_{\text{annual}} - \text{MR}_{\text{annual}}) > 0, \text{GR}_{\text{annual}} = 0.2 * (\text{GPP}_{\text{annual}} - \text{MR}_{\text{annual}})$$

$$\text{If } (\text{GPP}_{\text{annual}} - \text{MR}_{\text{annual}}) = 0, \text{GR}_{\text{annual}} = 0$$

$$\text{If } (\text{GPP}_{\text{annual}} - \text{MR}_{\text{annual}}) < 0, \text{GR}_{\text{annual}} = \text{GPP}_{\text{annual}} - \text{MR}_{\text{annual}}$$

Performance indicators

A) Global assessment (Heinsch et al., 2006). The error between annual GPP computed from NASA's Data Assimilation Office's (DAO/ GMAO) and tower-based meteorology is 28%, indicating that NASA's global meteorology plays an important role in the accuracy of the GPP algorithm. Approximately 62% of MOD15-based estimates of LAI were within the estimates based on field measurements, although remaining values overestimated site values. Land cover presented the fewest errors, with most errors within the forest classes, reducing potential error. MODIS GPP overestimates tower-based calculations by 20%-30%. Seasonally, summer estimates of MODIS GPP are closest to tower data, and spring estimates are the worst, most likely the result of the relatively rapid onset of leaf-out. Current MODIS GPP algorithm shows reasonable spatial patterns and temporal variability across a diverse range of biomes and climate regimes. Efforts are needed to isolate particular problems in specific biomes.

B) Global GPP/NPP assessment (Turner et al., 2006). Eddy Covariance flux measurements must be scaled over areas on the order of 25 km² to make effective comparisons to the MODIS products. MODIS products were compared against ground-based and spatially-scaled estimates of NPP/GPP using the Biome-BGC carbon cycle process model and Landsat auxiliary data. Outputs from both were compared at 9 sites varying widely in biome type and land use (arctic tundra, boreal forest, temperate hardwood forest, temperate conifer forest, tropical rain forest, tallgrass prairie, desert grassland, and cropland). MODIS products showed no overall bias, but they tended: a) to overestimate at low productivity sites — often because of artificially high values of MODIS FPAR, and b) to underestimate in high productivity sites — often a function of relatively low values for vegetation light use efficiency in the MODIS GPP algorithm. A global network of sites where both NPP and GPP are measured and scaled over the local landscape is needed to more comprehensively validate the MODIS NPP and GPP products and to potentially calibrate the MODIS NPP/GPP algorithm parameters.

C) Dry Sahel (Sjöström et al., 2013). Overall, seasonality was well captured but MOD17A2 GPP was underestimated for the dry sites located in the Sahel region. ϵ_{max} calculated from tower data was higher than the prescribed in MOD17A2. This, in addition to uncertainties in fraction of



absorbed photosynthetically active radiation (FPAR) explains some of the underestimations. The results suggest that improved quality of driver data, but primarily a readjustment of the parameters in the biome parameter look-up table (BPLUT) may be needed to better estimate GPP for African ecosystems in MOD17A2.

D) Dry Australia (Kanniah et al., 2009). GPP for C5 showed much lower values (RPE 25%) than actual measurements. Recalculation of MODIS GPP using site specific input parameters indicated that MODIS FPAR was the main reason for the differences between MODIS and tower derived GPP followed by LUE and meteorological inputs. The early initiation of the growing season calculated by the MODIS algorithm was improved when the vapor pressure deficit (VPD) function was replaced with a soil water deficit function. The results of this study however, reinforce previous findings in water limited regions, like Australia, and incorporation of soil moisture in a LUE model is needed to accurately estimate the productivity.

E) Tropical monsoon regions (Gebremichael and Barros, 2006). GPP products, available at 8-day and 1-km resolutions, were evaluated in two representative tropical ecosystems: a mixed forest (MXF) site in the humid tropics (the Marsyandi river basin in the Nepalese Himalayas), and an open shrubland (SHR) site in a semi-arid region (Sonora river basin in northern Mexico). The MODIS-GPP products were compared against simulations made with a process-based biochemical-hydrology model (LEHM) driven by flux tower meteorological observations. Temporal trajectories of vegetation indices and GPP products are consistent between the model and the algorithm. There is a positive bias in the humid mixed forest biome, and a negative bias in the semiarid open shrublands. The bias between the GPP estimates using DAO and tower meteorology is $-2.77 \text{ gC/m}^2/\text{day}$ (i.e., -77% of the mean of the tower-based GPP) in the humid ecosystem, and $0.33 \text{ gC/m}^2/\text{day}$ (i.e., 18% of the mean of the tower-based GPP) in the semiarid one. Analysis of the temporal evolution of the discrepancies between the model and the MODIS algorithm points to the need for examining the light use efficiency parameterization, especially with regard to the representation of nonlinear functional dependencies on vapor pressure deficit (VPD), photosynthetically available radiation (PAR), and seasonal evolution of the productive capacity of vegetation as influenced by water stress.

E) Forests (Tang et al., 2015). Overall, the site-specific evaluation of multi-year mean annual GPP estimates indicates that the current MODIS product works more significantly for deciduous broadleaf forest (DBF) and mixed forest (MF), less for evergreen needleleaf forest (ENF), and least for evergreen broadleaf forest (EBF). Except for the tropical forest, MODIS estimates could capture the broad trends of GPP at an 8-day time scale for the other sites. At the seasonal time scale, the highest performance was observed in ENF, followed by MF and DBF, and the least performance was observed in EBF. Trend analyses also revealed the weak performance in EBF and DBF. This study suggested that current MODIS GPP estimates still need to improve the quality of different upstream inputs in addition to the algorithm for accurately quantifying forest production.

G) Croplands (Xin et al., 2015). Model parameterization of the maximum light use efficiency (ϵGPP^*) varies considerably for croplands in agricultural studies at different scales. In this study, we evaluate cropland ϵGPP^* in the MODIS Gross Primary Productivity (GPP) model (MOD17) using in situ measurements and inventory datasets across the Midwestern US. Our results are in line with recent studies and imply that cropland GPP is largely underestimated in the MODIS GPP products for the Midwestern US. Our findings indicate that model parameters (primarily ϵGPP^*) should be carefully recalibrated for regional studies (Chen et al., 2011) and field-derived



ϵ GPP* can be consistently applied to large-scale modeling as we did here for the Midwestern US.

BEAMS (Biosphere model integrating Eco-physiological And Mechanistic approaches using Satellite data)

Source: (Sasai et al., 2005).

BEAMS runs at the monthly resolution and includes a stress calculation method for the LUE concept based on a photosynthesis model and a stomatal formulation. It requires both satellite and climate data. The stress scalar is computed using a Photosynthesis model and a canopy conductance formulation (Figure 26). BEAMS requires a large number of parameters (

Parameter	Temporal Resolution ^a	Spatial Resolution ^b	Details
Temp, Prec, VP	m	0.5 × 0.5 deg	CRU-TS2.0 dataset
SOL, NSW, NLW, WND	d	2.5 × 2.5 deg	NCEP/NCAR reanalysis
fAPAR, LAI	m	0.5 × 0.5 deg	FPAR/LAI derived from GIMMS NDVI data set ^c
Land cover map	c	1.0 × 1.0 deg	NDVI-derived land cover classification ^d
Soil texture, depth	c	1.0 × 1.0 deg	FAO soil texture groups
Elevation	c	10 × 10 min	U. S. Navy (FNOC) 10-minute elevation

^aAbbreviations: m, monthly; d, daily; c, constant.

^bAbbreviations: deg, degree; min, minute.

^cGlobal Inventory Monitoring and Modeling Studies NDVI data set [Myneni et al., 1997a, 1997b; Zhou et al., 2001; Nemani et al., 2003].

^dOne degree land cover map derived from AVHRR data [DeFries and Townshend, 1994].

Figure 27).

$$\text{GPP} = \text{PAR} * \text{FPAR} * \text{LUE}_{\text{max}} * \text{Ph}_s$$

$\text{Ph}_s = \text{P}/\text{P}_{\text{max}}$, i.e. the actual/maximum photosynthesis ratio. Ph_s depends on air temperature, air relative humidity, soil moisture and CO_2 concentrations. All these factors control the photosynthesis rate and its departure from optimum conditions.

NPP is computed as

$$\text{NPP} = \text{GPP} - \text{R}_a$$

R_a is the autotrophic respiration which is estimated using a carbon cycle submodel based on the Century model (Parton, 1993). BEAMS simulates mechanistically fluxes of GPP in different pools (biomass pools, litter pools and soil organic pools) and is allocated into leaf, stem and root components by an empirical equation using climate parameters. In BEAMS, the R_a of leaves, stems and roots consists of maintenance and growth respiration. Maintenance respiration is modeled in proportion to biomass with temperature dependence ($Q_{10} = 2$), while growth respiration is modeled in proportion to the potential NPP.

NEP is finally estimated simulating the litter fall and soil decomposition dynamics. Soil decomposition is parameterized taking into account the impact of soil moisture dynamics on the soil decomposition. Soil moisture dynamics is simulated using a hydrological submodel based on the BIOME3 model (Haxeltine and Prentice, 1996).



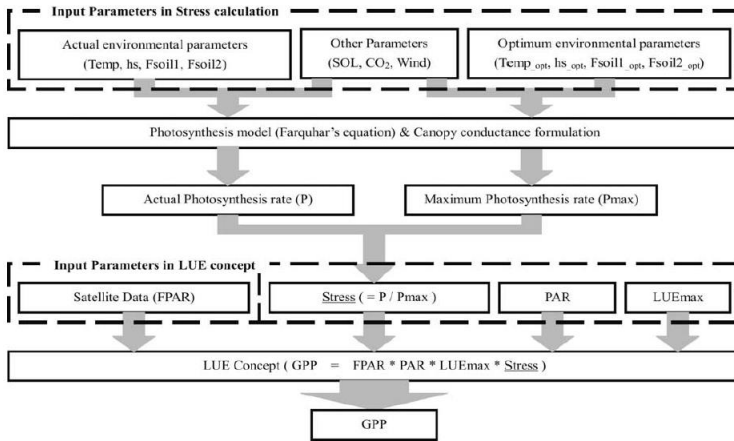


Figure 26. Schematic diagram of the BEAMS model (taken from Sasai et al. (Sasai et al., 2005)).

Parameter	Temporal Resolution ^a	Spatial Resolution ^b	Details
Temp, Prec, VP	m	0.5 × 0.5 deg	CRU-TS2.0 dataset
SOL, NSW, NLW, WND	d	2.5 × 2.5 deg	NCEP/NCAR reanalysis
fAPAR, LAI	m	0.5 × 0.5 deg	FPAR/LAI derived from GIMMS NDVI data set ^c
Land cover map	c	1.0 × 1.0 deg	NDVI-derived land cover classification ^d
Soil texture, depth	c	1.0 × 1.0 deg	FAO soil texture groups
Elevation	c	10 × 10 min	U. S. Navy (FNOC) 10-minute elevation

^aAbbreviations: m, monthly; d, daily; c, constant.

^bAbbreviations: deg, degree; min, minute.

^cGlobal Inventory Monitoring and Modeling Studies NDVI data set [Myneni et al., 1997a, 1997b; Zhou et al., 2001; Nemani et al., 2003].

^dOne degree land cover map derived from AVHRR data [DeFries and Townshend, 1994].

Figure 27. Input datasets used in BEAMS (taken from Sasai et al. (Sasai et al., 2005)).

EC-LUE model (Eddy Covariance – Light Use Efficiency model)

Source: (Yuan et al., 2007).

$$GPP = PAR * FPAR * LUE_{max} * \min(T_s, W_s) \quad [\text{Eq. 14}]$$

In its original formulation, FAPAR is computed as

$$FAPAR = 1.24 * NDVI - 0.168 \quad [\text{Eq. 15}]$$

The EC-LUE model assumes the Liebig's law, in which LUE is controlled by the minimum value of a set of scalar factors acting at the same time. In the EC-LUE model, a temperature-based and water-based scalar are considered.

T-scalar. It is computed following the formulation adopted in the Terrestrial Ecosystem Model TEM (Raich, 1991), as

$$T_s = \frac{(T - T_{min})(T - T_{max})}{[(T - T_{min})(T - T_{max})] - (T - T_{opt})^2} \quad [\text{Eq. 16}]$$



Table 12. Temperature thresholds used for computing the T-scalar parameter in the VPM model.

Vegetation type	Tmin	Topt	Tmax	Reference
Evergreen forest	2.5	27.5	47.5	(Raich, 1991)
Evergreen needleleaf forest	0.0	20.0	40.0	(Xiao et al., 2004)
Temperate forest	-2.0	22.5	44.0	(Raich, 1991)
Tropical forest	2.0	28.0	48.0	(Xiao et al., 2005)
Xeromorphic forest	-1.5	22.5	48.5	(Raich, 1991)
Arid shrubland	-3.0	25.0	48.5	(Raich, 1991)
Savanna	-1.0	30.0	49.5	(Raich, 1991)
Grassland	1.0	30.0	48.0	(Raich, 1991)
Maize	10	28.0	48.0	(Kalfas et al., 2011)
Soybean	-1.0	28.0	50.0	(Wagle et al., 2015)

W-scalar. It is computed as the Evaporative Fraction, as:

$$W_s = EF = \frac{LE}{(LE + H)} = \frac{1}{1 + \beta}$$

[Eq. 17]

Being, LE the latent heat flux (MJ/m².day), H the sensible heat flux (MJ/m².day), and β the Bowen ratio (non-dimensional). The evaporative fraction can be computed from satellite data (see for example the Wang's or Venturini's approaches (Venturini et al., 2008; Wang et al., 2006))

VPM (Vegetation Photosynthesis Model)

Source:(Xiao et al., 2004).

VPM estimates GPP using satellite data from MODIS and SPOT-Vegetation sensors. It uses EVI to account for APAR and, functions of optimum temperature, water and leaf phenology to scale down the maximum LUE. Soil water condition is represented using a Land Surface Water Index (LSWI) that is calculated from the near infrared -*nir*- and shortwave infrared -*swir*- spectral bands.

$$GPP = PAR * FPAR_{PAV} * LUE_{max} * (T_s * W_s * P_s)$$

T-scalar. See [Eq. 16].

W-scalar. It is computed as

$$W_s = \frac{1 + LSWI}{1 + LSWI_{max}}$$

[Eq. 18]

$$LSWI = \frac{nir - swir}{nir + swir}$$

[Eq. 19]

where



LSWI = Land Surface Water Index,
 LSWI_{max} = maximum value of LSWI reached during the growing season.

Other W-scalar formulations have been proposed by others using LSWI (Gao et al., 2014; Jin et al., 2015) or the Vapour Pressure Deficit of the air (Nguy-Robertson et al., 2015).

Phenology scalar, it is computed as:

$$P_s = \begin{cases} \min\left\{1, \frac{1 + LSWI}{2}\right\}, & \text{for deciduous} \\ 1, & \text{for perennial} \end{cases}$$

[Eq. 20]

VPM does not track accurately the seasonal variability of GPP in tropical evergreen forest where old-growth trees remain a dense canopy (phenology is not well characterized) and develop deep roots to absorb underground water during the dry season.

VI-based models for estimating GPP

TG model (Temperature and Greenness model)

Source: (Sims et al., 2008)

It is an empirical model based entirely on remote sensing data. It rests on simple relationships between Land Surface Temperature (LST) and the Enhanced Vegetation Index (EVI), both retrieved from MODIS (Sims et al., 2008). The TG model does not use weather variables nor PAR measurements as inputs, because Sims et al. (2008) found for North America that LST is strongly correlated with PAR and VPD measurements. GPP is then estimated as a product of scaled values of LST and EVI. The TG model has been proposed to be used to estimate ecosystem productivity when there is no prior knowledge about the site (Wu et al., 2010b).

Overall, the TG model agreed well ($R^2 = 0.79-0.94$) with nine site measurements in North America (Sims et al., 2008), and provided substantially better predictions of GPP than did the MODIS-GPP product. However, both models resulted in poor predictions for sparse shrub habitats where solar angle effects on remote sensing indices were large (Sims et al., 2008).

$$GPP = (EVI_{sc} * LST_{sc}) * m$$

[Eq. 21]

being,

$$EVI_{sc} = EVI - 0.1$$

[Eq. 22]

$$LST_{sc} = \min\left[\left(\frac{LST}{30}\right); 2.5 - 0.05 * LST\right]$$

[Eq. 23]

The slope m is computed from Eddy-covariance GPP measurements and $EVI_{sc} * LST_{sc}$ values, and varies site-by-site. Sims et al. (2008) found a close correlation with the annual mean of nighttime LST values, probably because nighttime values represent a better estimate of the baseline temperature that regulates plant phenology.

$$m = a - b * LST_{an}$$

being LST_{an} the annual mean nighttime LST. The $a-b$ pair values optimized for deciduous and evergreen sites were 2.49-0.074, and 2.10-0.0625 respectively.



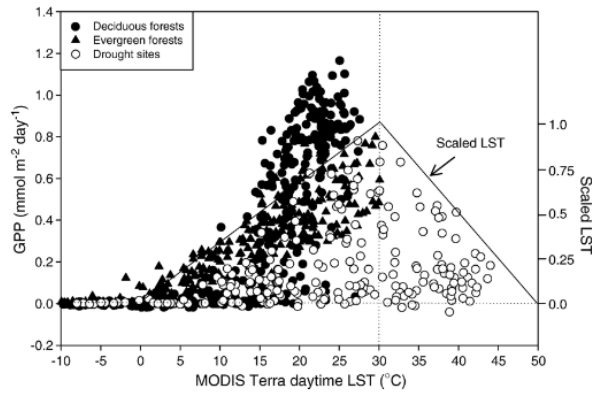


Figure 28. Actual GPP measurements as a function of Land Surface Temperature (LST) in different vegetation-type systems (taken from Sims et al. (2008)).

GR model (Greenness and Radiation Model)

Sources: (Gitelson et al., 2006, 2012; Peng et al., 2011; Wu et al., 2011).

Peng et al. (Peng et al., 2011) provide the theoretical background behind the GR model, and test its performance using different satellite-based vegetation indices extracted from ground-based reflectance measurements in maize (SR, NDVI, EVI2, WDRVI, CI_{green} , $CI_{red-edge}$). The chlorophyll indices and the simple ratio (SR) were the best predictors of GPP.

$$GPP = VI_{Chl} * PAR$$

[Eq. 24]

In which, VI_{Chl} is a function of a vegetation index.

According to (Wu et al., 2011),

$$GPP_{month} = m * (EVI * PAR)$$

[Eq. 25]

where

$$m = f(EVI_{max} - EVI_{min}, T_sd)$$

VI model (Vegetation Index Model)

Source: (Wu et al., 2010c).

It is based on a VI*VI approach. GPP is estimated from ground PAR measurements and the combination of two vegetation indices (i.e. PAR * Vegetation index * Vegetation index). In this model, vegetation indices are assumed to be well surrogates of FPAR and actual LUE values.

$$GPP = PAR * FPAR(VI) * LUE(VI)$$

[Eq. 26]

Among the different tests performed by (Wu et al., 2010c), the PAR*EVI*EVI combination resulted in the best configuration for explaining GPP in maize (Wu et al., 2010c), wheat (Wu et al., 2010b) and deciduous forests (Wu et al., 2010a). However, the application of the VI model may be problematic under drought conditions because in those cases VIs usually fail in explaining light use efficiency values.

TGR (Temperature and Greenness Rectangle)

Source: See Yang et al. (Yang et al., 2013) for a detailed description.



MOD-PCM

Source: (Gao et al., 2014)

The general equation of PEMs (see [Eq. 1]) can be rewritten into:

$$GPP = (LUE_{max} * pPAR_{max}) * (FPAR * pPAR_t) * f = PC_{max} * PC_t * f$$

[Eq. 27]

where, PC_{max} represents the maximum photosynthetic capacity, PC_t is a down-regulated factor that varies with the absorbed PAR, which can be used to represent the variability of photosynthetic capacity under different growth stages, and f is a downward regulating factor for LUE_{max} ranging from 0 to 1 under various environmental limiting conditions. The term $pPAR$ represent the maximum values of incoming PAR that may occur when concentrations of atmospheric aerosols and gases are minimal.

This model states that the photosynthetic capacity depends on the amount of photosynthetic apparatus within a plant community and can be directly expressed by the total content of canopy chlorophyll which can be estimated from satellite-based vegetation indices as the EVI. Additionally, soil moisture is considered as the primary limiting factor of GPP, so [Eq. 27] is finally converted into:

$$GPP = PC_{max} * EVI_s * W_s$$

[Eq. 28]

where, EVI_s represents the variability of PC, and W_s indicates the moisture conditions that downward regulate PC (it is computed using a LWSI-based approach, see .

